Grid Controllability Aware Optimal Placement of PMUs with Limited Input Current Channels

Akash Kumar Mandal, Swades De, and Bijaya Ketan Panigrahi

***Abstract*—This paper proposes a novel approach for optimal placement of phasor measurement units (PMUs) targeting smart grid controllability under perturbed system conditions while ensuring system observability. In determining the optimal number of required PMUs, as a practical consideration, PMUs are considered to have limited number of input channels. To achieve this optimality objective, a weighted least square optimization problem with a continuous relaxation is considered for the discrete binary constraint. An information-theoretic viewpoint is taken for characterizing the robustness of grid estimation at the phasor data concentrator. A perturbation-robust algorithm is developed for a global optimal solution for PMU placement. The efficacy of the proposed smart grid monitoring approach is validated on IEEE 6, 14, 30, 57, and 118-bus systems. The results demonstrate that, unlike the conventional system observability aware PMU deployment, the proposed strategy ensures system controllability under generic perturbation conditions while maintaining the grid observability at $\approx 100\%$, a minimum mean squared error $\approx 10^{-3}$, and mutual information between estimated and measured attributes close to 1 in all test cases.**

***Index Terms*—Grid controllability, limited input current channels, optimal PMU placement, perturbation, phasor measurement unit (PMU)**

I. Introduction

Due to the increased interfacing of power electronic devices in the grid (for the purpose of voltage regulation and stability, power flow control, dynamic reactive power compensation, integration of renewable energy sources, improving system reliability and flexibility, fault current limitation, load balancing and power flow optimization, etc.) and the increasingly deregulated electricity market, modern electric power grids are forced to operate closer to their stability and thermal limits [1]. Proliferation of power electronic switching based loads and sources have also led to manifold increase of sustained as well as sporadic perturbations in the recent years [2]. Prevalence of such perturbed system states motivates the need for a revised instrumentation for real-time monitoring and estimation in the modern power system for its reliable operation and control [3].

The advanced instrumentation of the power grid includes the integration of phasor measurement units (PMUs), which provide real-time measurements of critical grid attributes across different nodes for enhanced monitoring and control [4], [5]. These devices communicate their measurements to a local phasor data concentrator (PDC), for monitoring and control by running estimations and predictions under various system conditions. System state estimation at the PDC is compounded by the errors due to electromagnetic noise from power lines during PMU data transmission [6]. Therefore, owing to high installation and maintenance costs of the PMUs along with the requirement of accurate system state estimation, optimal PMU placement strategy is highly important for providing an economic and effective monitoring solution. Moreover, PMU deployment strategy also needs to ensure accurate system state estimation at the PDC under perturbed grid conditions.

In the scope of this work, controllability is defined as the ability of the optimally deployed PMUs with limited input current channels to estimate a perturbed grid health at the PDC within acceptable error bounds. We intend to pursue this optimal PMU placement aiming to achieve grid controllability under perturbation while ensuring robust observability.

A. Literature Review and Motivation

The related work on smart grid monitoring instrumentation can be broadly divided into three sets. The first set [7]–[10] present various strategies for optimal PMU placement at minimized deployment cost while maintaining a basic grid observability. These studies did not consider the practical constraint of limited input current channels of the PMUs. The research in [11]–[13] proposed the aspect of grid observability and fault visibility using optimally deployed limited current channel PMUs. They did not consider the notion of grid controllability owing to proper system state reconstruction at the PDC under perturbed system conditions. The work in [14] demonstrated the impact of erroneous system state measurement/reconstruction after pruning, on the observability attained using the PMU placement optimization, while limiting the current channel capacity per PMU. However, the system states arising from perturbed grid conditions were not considered. As a consequence, the applicability of such approaches is limited in modern grids, where renewable penetration causes sustained oscillations. Therefore, optimized PMU deployment solutions rendered by these existing approaches need to be revisited to address the practical system and placement constraints.

The second set of work employ different statistical approaches [15]–[19], and evolutionary algorithms [20]–[22], for optimal PMU placement in various grid topologies. They aim at devising unique placement solutions with time constraints. Though time complexity reduction in optimal PMU placement is an important objective, the key practical aspects, namely, realistic PMU capabilities, accounting for grid perturbation, and grid controllability beyond only observability, require fur-

A. K. Mandal, S. De, and B. K. Panigrahi are with the Department of Electrical Engineering and Bharti School of Telecommunication, IIT Delhi, New Delhi 110016, India (e-mail: {akash.kumar.mandal, swadesd, bkpanigrahi}@ee.iitd.ac.in). A preliminary version of this work was presented in IEEE International Conference on Energy Technology for Future Grids (ETFG) 2023, Wollongong, Australia.

ther research attention. The research in [23] employed a judicious combination of branch and bound algorithm, successive quadratic programming, and interior point methods for finding optimal PMU placement solution ensuring maximum measurement redundancy in reduced number of PMUs. However, optimal PMU placement for controllability of perturbed power networks has not been discussed thus far in the literature. Also, the consideration of efficient state estimation at the PDC in the optimization formulation for the placement of single current channel PMUs in perturbed power networks has remained unaddressed. Such aspect becomes crucial for providing an accurate data-based control in perturbed grids [24].

The final set [25]–[28] look into the optimal PMU placement considering different system adversities. These works analyze the PMU placement variations under different line and PMU outages. The studies in [29] and [30] analyze a multi-stage PMU installation process for co-phasing while ensuring complete system observability. The works in [31], [32] further analyze the use of the installed PMUs in outage detection in power networks. Though these studies demonstrate some variability on the optimal placement by considering a revised grid connectivity, such outage scenarios may not occur frequently in the grid. Moreover, the objective of wide area monitoring systems is to avoid such outages. Additionally, with the notion of micro-grid, perturbed grid states are more predominant now-a-days. Therefore, understanding the perturbed grid states, between the two extreme states, namely, ideal and grid outage states, is of current interest. This allows wideband stability analysis and appropriate control in ensuring the operational stability of perturbed power networks [33].

In our recent preliminary studies [34], we considered optimal PMU placement under perturbed grid states for various standard IEEE test systems and analyzed the involved optimization problem. However, the impact of limited input current channels in practical PMUs on the estimation accuracy of real power networks under perturbation was not considered. In other words, an analysis of optimum placement of PMUs with limited input current channels for monitoring perturbed grid conditions and thus ensuring controllability is yet to be reported in the literature.

B. Contributions and Significance

As an advance, this paper utilizes the perturbation-immune optimal placement of PMUs with limited input current channels from a redefined notion of grid controllability developed in [34], and augments it with an approach for optimal estimation of the perturbed grid states at the data collector. This study assumes additional importance due to rapid increase in grid non-linearity, arising from the incorporation of power electronic devices. In view of the lacuna in the literature on practical instrumentation of smart grid for monitoring and controllability under perturbations, we revisit the optimum PMU deployment strategy. The key contributions of this work are as follows:

1) The notion of line observability reward and node weight vector are proposed for efficient grid health characterization under random perturbations.
2) A minimum cost constrained quadratic objective problem over a bounded decision domain is formulated, which employs a polynomial grid observability constraint while considering the presence or absence of zero injection bus (ZIB), for ensuring grid controllability under perturbations.
3) For ensuring an accurate estimation of grid states at the PDC using data from optimally deployed PMUs in perturbed power networks, an information theoretic measure is considered in the PMU placement optimization. Further, a penalty-aware perturbation-robust optimal PMU placement algorithm is presented to solve the final non-convex optimization problem.
4) The two-stage optimization problem is solved for perturbed grid scenarios in an IEEE 6-bus system, to highlight the trade-off from relaxing the assumption of sufficient input channels, and a revised PMU placement vector is obtained to deal with perturbations. IEEE 14, 30, 57, and 118-bus systems are considered for further validation, establishing the importance of the proposed perturbation-robust PMU placement strategy.

Simulation results demonstrate that the proposed grid controllability-aware PMU deployment is able to capture the grid health under perturbations, which is otherwise not possible in the existing conventional deployment strategy. With the proposed approach, a robust grid estimation at the PDC is demonstrated with a significantly reduced minimum mean squared error (MMSE) in the estimated values of the grid health attributes at pseudo-monitored nodes. Also, using the proposed deployment strategy, mutual information between the estimated and measured attribute vectors increases to unity, thus ensuring sufficient grid observability under perturbed grid scenarios. Furthermore, the contingency analysis assures reinforced controllability and observability rendered by the proposed strategy under PMU outage and line loss conditions.

Remark 1. *It is notable that, consideration of faults or loss of a PMU alone does not model the real operating conditions of the grid, which are majorly attributed to the wideband perturbations that are present in the power network, arising by the virtue of high renewable penetration. One of the core contributions of this research is in establishing an optimal PMU deployment policy for ensuring PMU data-based controllability of perturbed power networks.*

C. Industry Relevance of the Proposed Controllability-Aware PMU Placement Optimization

According to North American Electric Reliability Corporation's (NERC) 'Reliability Guideline for PMU Placement and Installation' [35], the installation of PMU follows 'standard utility practice' for planning, design, and commissioning. The planning stage involves determination of measurements to be considered, signals required to achieve those measurements, and the signal sources for the PMUs. Therefore, PMU installation, commissioning, and maintenance guidelines in [36], [37], efficient deployment of optimum number for PMUs is considered a practical concern in all electric grids, utility providers,

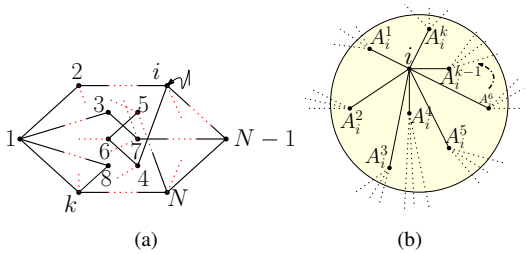

(a) (b)

Fig. 1: (a) N-node smart grid network graph, (b) incidence diagram for node i with k incident lines.

and electricity regulatory bodies, such as Federal Energy Regulatory Commission (United States), Canadian Electricity Association, Central Electricity Regulatory Commission (India), State Grid Corporation of China, National Electric System Operator (Brazil), Eskom (South Africa), Australian Energy Market Operator, European Network of Transmission System Operators for Electricity,Tokyo Electric Power Company, etc. Also, it is worth mentioning that optimum state estimation of future grids under perturbed system states is still a challenging aspect in robust grid operation and monitoring.

As outlined by NERC, more than 90% of the real-time as well as non-real time PMU aspects involve grid observability and state estimation under perturbed conditions using PMUs [35], which has not been discussed in the present state-of-the-art. Further, one of the key aspects involved in signal monitoring as well as equipment design is concerned with the number of input channels in the PMU. Based on 'NASPI Synchrophasor Starter Kit' [38], limited input channels may lead to multiple PMU installation at one bus for complete monitoring of the situation. This strengthens the importance of the issue of limited input channels presented in this work.

From the above discussion, it is established that optimal deployment of PMUs with limited input current channels is a pertinent problem considered by the utilities. Moreover, it is specifically discussed under 'Some Additional Myths and Misconceptions' subsection of [38], *synchrophasor visualization in conventional power grids is far from mature*. In other words, the domain is not yet sufficiently explored industrially.

D. Paper Organization

The paper layout is as follows: Section II presents the system model, Section III contains the optimization problem formulation for the proposed grid perturbation-robust PMU placement strategy and definitions of the involved parameters, followed by the results and conclusion in Sections IV and V.

II. System Model for Optimal PMU Placement

Consider a power grid with a set of buses indexed by $\mathscr{N} := \{1, 2, \cdots, N\}$. The buses are connected through a set of transmission lines $\mathscr{L} \subset \mathscr{N} \times \mathscr{N}$, i.e. , bus i is connected to bus j iff $(i, j) \in \mathscr{L}$. Accordingly, $\mathbf{A}_i$ is the set of buses incident to bus i, with the element j represented as A_i^j, such that $\|A_i\| = k_i$ is its incidence order as shown in Fig. 1(b). Further, let us define the grid incidence matrix $\mathbf{A} = [a_{i,j} | i, j \in \mathscr{N}]$, such that $a_{i,j} = 1$, iff nodes i and j are connected, and 0 otherwise. Controllability in this work implies the ability to reconstruct the system image at the PDC for monitoring under perturbed system conditions. We consider voltage and current phasor perturbations while proposing the perturbation-robust optimal PMU placement strategy. Perturbations amounting to Δv_i, $\Delta \phi_i$, $\Delta i_{i,j}$, and $\Delta \delta_{i,j}$ against the i-th node's steady state voltage magnitude v_i, voltage phase ϕ_i, current magnitude $i_{i,j}$, and current phase $\delta_{i,j}$ is considered in the mentioned order, as shown in Fig. 1(a), and propagation through all incident lines to node i is considered.

All PMUs are considered to have a limited number of input current channels, typically 1, that is less than the minimum node order of the grid. This consideration ensures to critically base the estimation error metric on the robustness of the proposed PMU placement and estimation approach without gaining any measurement aid from the PMUs with multiple input current channels. It may be noted that, our formulations do not restrict the use of PMUs with multiple input current channels, as they do not change the idea contribution in our research. A 50 Hz grid is considered, where the input voltage and current readings are recorded at $19,200$ samples per second and reported at 200 fps to the PDC [39]. The PMUs monitor 3-phase voltages, 3-phase currents, corresponding voltage and current phasors, neutral and positive sequence voltages, frequency, and rate of change of frequency. It is expected that PDC along with supervisory control and data acquisition take necessary control actions based on the PMU data at the local and central data center.

Remark 2. *The notion of controllability posed in this work relates in a modified way with the known definition of controllability. For a system to be controllable, it must be estimated correctly at the data center first. This is because, in control engineering, the error between the output of the actual system and the response of its image system, after applying the control signal, is used as a measure. This error signal is fed back to the controller to ensure robust control of the system. Thus, without proper system information, owing to imperfect system reconstruction, accurate control action would not be possible.*

III. Optimal PMU Placement Analysis

This section presents the prerequisites for the controllability-aware optimal PMU placement problem, followed by the optimization problem formulation. The optimal solution to the problem is achieved using our proposed Algorithms 1 and 2, as detailed subsequently. A broad overview of the steps involved in the proposed framework is depicted in Fig. 2. The subsequent formulations model the power network perturbations using 'small-signal perturbation modeling' and employs an information theoretic viewpoint in evaluating efficient grid health estimation using the data from optimally deployed PMUs. For completeness, we propose an efficient approach to attain an optimal solution for the PMU placement in perturbed power networks.

A. Line Observability Reward Formulation

Let us define a variable z_i s.t, $z_i = 1$ or 0 implies the presence or absence of PMU at the i-th bus respectively. Let

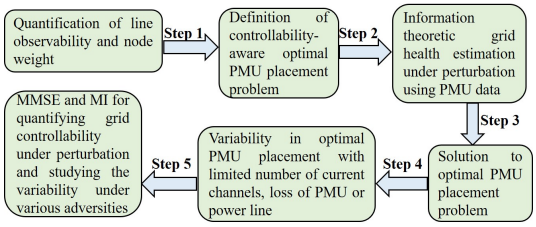

Fig. 2: Work flow of grid controllability-aware PMU placement.

R out of N grid nodes have a PMU, with the PMU installed at the i-th node having l_i input channels with node order k_i, s.t. $l_i < k_i$. If $\Pr(\mathrm{L}_{i,j})$ signifies the probability that link i-j gets monitored, then we have $\Pr(\mathrm{L}_{i,j}) \triangleq \mathrm{I}\left(\mathrm{L}_{i,j}=1\right)(z_i x_i + z_j x_j)$, where $\mathrm{I}(\mathrm{L}_{i,j}=1)$ is a binary indicator function that takes 1 iff node i and j are connected and x_i denotes the random variable representing the probability of link i-j getting monitored by the PMU installed at node i. The randomness results from random selection of lines to be monitored using a PMU with limited input channels, as there is no defined norm for such a selection. Therefore, the average reward for observing the link i-j is defined as $\mu_{i,j} = c_{i,j}\mathbb{E}[\Pr(L_{i,j})] = c_{i,j}\mathbb{E}[\mathrm{I}(L_{i,j}=1)(z_i x_i + z_j x_j)]$, where $c_{i,j}$ is the reward for observing link i-j, and relates to the importance of that node. Ideally, the desired probability of a line getting monitored is 1. Further, the order of installation also plays a role in defining this probability. For instance, if an input current channel from the PMU installed at node i is used, the channel availability for other incident lines to node i decreases to $l_i - 1$, and so on. Considering all such orders, the average line observability reward is

$$\begin{aligned}\mu_{i,j} =& c_{i,j}\mathrm{I}(L_{i,j}=1)(z_i\mathbb{E}[x_i] + z_j\mathbb{E}[x_j]) \\ =& c_{i,j}\mathrm{I}(L_{i,j}=1)(z_i S_i + z_j S_j)\end{aligned}$$

where $S_i = \mathbb{E}[x_i] = \sum_{x_i=1}^{l_i} x_i \frac{1}{k_i-(l_i-x_i)} = \frac{1}{k_i-l_i+1} + \frac{2}{k_i-l_i+2} + \cdots + \frac{l_i}{k_i}$. On simplifying, we get

$$\begin{aligned}S_i &= \frac{l_i}{k_i} + \frac{l_i-1}{k_i-1} + \cdots + \frac{1}{k_i-l_i+1} = 1 - \sum_{j=1}^{l_i-1}\frac{(k_i-l_i)}{k_i-j} \\ &\approx 1 - \int_0^{\frac{l_i-1}{k_i}} \frac{(k_i-l_i)}{1-x}dx = 1-(k_i-l_i)\ln\left(1-\frac{l_i-1}{k_i}\right).\end{aligned} \tag{1}$$

S_i denotes the average number of input current channels monitoring the link i-j using a PMU installed at node i. Thus, the average line observability reward matrix is given as

$$\mathbf{A}_l = \begin{bmatrix}\mu_{1,1} & \mu_{1,2} & \cdots & \mu_{1,N} \\ \vdots & \vdots & \ddots & \vdots \\ \mu_{N,1} & \mu_{N,2} & \cdots & \mu_{N,N}\end{bmatrix} = \mathbf{c}\odot\mathbf{A}\odot\mathbf{d} \tag{2}$$

where $\odot$ denotes a Hadamard product, $\mathbf{A}$ is the grid incidence matrix, $\mathbf{c}$ is the reward matrix with the (i,j) entry defined as $c_{i,j}$, and $\mathbf{d} = \mathbf{v}^T\mathbb{1} + \mathbf{I}\mathbf{v}$ such that $\mathbb{1} = [1,1,\cdots,1]_N^T$, $\mathrm{I} = \mathrm{diag}\left(\mathbb{1}_1, \mathbb{1}_2, \cdots, \mathbb{1}_N\right)$ is a matrix of dimension $N \times N$ with its i-th diagonal entry $\mathbb{1}_i$ being a vector of ones having a zero only at i-th position. Using the above formulations in (2), we get $A_l = c \odot A \odot \left(\mathbf{v}^T\mathbb{1} + \mathbf{I}\mathbf{v}\right)$. Further, $\mathbf{v} = \mathbf{S}\mathbf{z}$ is defined for the sake of concise representation, such that $\mathbf{S}$ is diagonal, and the (i,i) entry in $\mathbf{S}$ is defined as S_i, as in (1). Let the node weight vector be defined as $\boldsymbol{\omega}$ with ω_i the weight for the i-th node. Then, the aggregate grid observability index (AGOI) is defined as $\boldsymbol{\omega}^T c \odot A \odot \left(\mathbf{z}^T\mathbf{S}^T\mathbb{1} + \mathbf{I}\mathbf{S}\mathbf{z}\right)\boldsymbol{\omega}$.

Remark 3. *It is worth noting here that, the node selection for PMU placement renders different node incidence order resulting from different number of lines incident to a node, consequently it affects the AGOI.*

Further, the importance of observing the link i-j stems from the Thevenin equivalent impedance between the nodes. The Thevenin equivalent impedance between node i-j $\forall i,j \in \mathscr{N}$ given by $\mathbb{Z}_{i,j}$ is calculated using the Z bus matrix algorithm in [40]. It gives a sense into the ability of a node pair to destabilize the network under perturbation, as can be inferred from (A6). In the scope of this work, we define $c_{i,j} = \frac{\mathbb{Z}_{i,j}}{\sum_{i=1}^{N}\mathbb{Z}_{i,j}}$, as the reward for observing link i-j. Further, controllability for the i-th node is defined as $o_i = \sum_{j\in\mathbf{A}_i}\mu_{i,j}$, with the controllability vector defined by $\mathbf{O}^T$. The definition of node weight vector by considering perturbations in the voltage magnitude of the concerned node is proposed in Lemma 1.

Lemma 1. *The weight of the j-th node is defined as*

$$\omega_j = \left(\sin(\omega t+\phi_j)\sum_{r=1}^{k_j} z_{j_r,j}^{-1}\right)\left(\sum_{r=1}^{k_j}\sin(\omega t+\phi_{j_r})z_{j_r,j}^{-1}\alpha_{j_r}\right)^{-1}$$

where $\Delta v_{j_r} = \alpha_{j_r}\Delta v_0$, where Δv_0 is the instability grid node voltage change and α_{j_r} is a constant of multiplication, $\omega = 2\pi f$ is the angular grid frequency, t represents time, $z_{i,j} = \sqrt{r_{i,j}^2 + x_{i,j}^2}$ is the impedance of link i-j, with $r_{i,j}$, and $x_{i,j}$ denoting the link resistance and reactance, respectively.

Proof. See Appendix A. □

In the scope of this work, we consider time-limited complex voltage perturbations to obtain the wideband perturbed system conditions, which are then modeled using the average line observability reward and the node weight vector, as defined above. The introduction of complex voltage perturbation in the network equations is detailed in the proof presented in Appendix A.

Remark 4. *Lemma 1 captures the node weight based on the proximity of its operating voltage to instability. Intuitively, for a node with operating voltage closer to instability, a direct PMU monitoring is necessary.*

B. Formulation of Optimal PMU Placement Problem

A quadratic minimization problem is formulated in $\mathbf{F}_1$ which aims at making the grid observable with minimum number of PMUs, and optimum network controllability based on maximizing the grid controllability under perturbation is ensured by maximizing $\mathbf{F}_2$ in (3) as follows

$$\begin{aligned}&\mathbf{F}_1 : \text{Min } \{\mathbf{z}^T\mathbf{C}_\mathrm{P}\mathbf{z} + \mathbf{G}(\mathbf{z})^T\mathbf{V}\mathbf{G}(\mathbf{z})\} \\ &\mathbf{F}_2 : \text{Max } \mathbf{O}^T\mathbf{c}\mathbf{O} \text{ s.t. } \mathbf{C}_1 : \mathbf{z} \in \mathscr{D}_R\end{aligned} \tag{3}$$

where constraint $\mathbf{C}_1$ refers to the first constraint outlining the possibility space of the variable $\mathbf{z}$ representing the presence of

PMU at N nodes, s.t. $\mathscr{D}_R := \left\{\mathbf{z} \in \{0,1\}^N \,\middle|\, \sum_{i\in\mathscr{N}} z_i = R\right\}$, $\mathbf{C_P} = c\mathbf{I_N}$, with c denoting the per PMU cost, $\mathbf{G(z)} = [g_1(\mathbf{z}), \cdots, g_2(\mathbf{z})]^T$, $\mathbf{V} = \mathbf{v}^T \odot \mathbf{I_N}$, with $\mathbf{v} = [v_1, \cdots, v_N]^T$ denoting the unobservability cost for the nodes $i \in \{1, \cdots, \mathrm{N}\}$, $\mathbf{O} = [o_1, o_2, \cdots, o_N]$, with $o_i = \sum_{j\in\mathbf{A}_i} \mu_{i,j}$, and $\mathbf{c} = [c_{i,j}]_{i,j\in\{1,\cdots,N\}}$, with $c_{i,j} = \frac{\mathbb{Z}_{i,j}}{\sum_{i=1}^{N}\mathbb{Z}_{i,j}}$, where $\mathbb{Z}_{i,j}$ denotes the Thevenin equivalent impedance of link i-j. This cost is set high to ensure a binary (0 or 1) PMU assignment to the respective buses. Motivated by the research in [41], in this work we define a polynomial observability function $g_i(\mathbf{z}) \in \{g_{i,\overline{ZIB}}(\mathbf{z}), g_{i,ZIB}(\mathbf{z})\}$ for node i, with the two functions capturing the aspect of not considering or considering the impact of zero injection bus (ZIB) respectively. Neglecting ZIB we have

$$g_{i,\overline{ZIB}}(\mathbf{z}) = \sigma_i - z_i - \sum_{j\in A_i} z_j,\ \forall i \in \{1, \cdots, N\} \tag{4}$$

where σ_i is the redundancy order for the i-th node, denoting total PMUs monitoring that node, and $\mathbf{A}_i$ is the set containing nodes incident to node i. A joint weighted optimization problem from (3) can be formulated as

$$(\mathbf{P}_1) : \text{Min J}(\mathbf{z}) = \mathbf{F}_1 - \lambda\mathbf{F}_2 \text{ s.t. } \mathbf{C}_1 \tag{5}$$

where $\lambda \in \{0, 1\}$ is a binary weight, outlining the choice seeking either a controllability-aware optimal PMU placement solution with $\lambda = 1$, or conventional optimality with $\lambda = 0$. It is notable that the controllability-aware optimization perspective dwells on optimum grid observability and control under perturbed grid conditions using limited number of practical PMUs with one input channel. Furthermore, ZIBs are the nodes that cause no current injection into the system. Thus, if all buses incident to a ZIB are observable except one, the unobserved bus can be made observable by applying KCL at the ZIB. Further, if all buses incident to the ZIB are observable except the ZIB, it can be made observable by applying KCL at the ZIB. Let t_i be a binary parameter taking 1 iff bus i is a ZIB, and $y_{i,j}$ be an auxiliary binary variable corresponding to bus i and j, such that $j \in \mathbf{A}_i$. If $Y_i = \{y_{i,j}\}$, then $\|Y_i\| = \|\mathbf{A}_i\| + t_i$. Therefore, the observability constraint defined in (4) modifies to (6) under the considerations of ZIB

$$g_{i,ZIB}(\mathbf{z}) = \sigma_i - z_i - t_i y_{i,i} - \sum_{j\in A_i} (z_j + t_j y_{i,j}) \tag{6}$$

with all notations as defined previously. Thus, the proposed PMU placement problem including ZIB can be given by updating $g_i(\mathbf{z})$ in (3) and substituting in (5).

The idea of robust grid health estimation at the PDC using PMU data is proposed next. Information theoretic metrics, such as MMSE in the estimated data at data collector and normalized mutual information about the pseudo-monitored nodes using the data from direct monitored nodes are quantified as the measures of robustness of the proposed strategy.

The optimization problem formulations in (3) target minimum-cost placement of PMUs in the power grid while simultaneously ensuring optimum network controllability under perturbation. The expressions (4) and (6) define polynomial observability functions in absence and presence of ZIBs, respectively, and (5) proposes the weighted joint optimization problem. All these formulations follow the first principles of mathematics, thus can be verified for correctness. Furthermore, the dimensional compatibility of all these formulations validates the mathematical correctness.

Remark 5. *It is worth highlighting that the quadratic formulation in* (3) *is different from any regression process of the form $y = f(x) + \epsilon$, where $f(\cdot)$ is found by minimizing the error ϵ. The formulation is in the quadratic form that achieves a unique optimal solution as a consequence of its convex structure.*

C. PMU Data Based Grid Estimation Under Perturbation

Under the established power system model, the power injection at bus k is approximated by

$$P_i = B_{i,i}\theta_i + \sum_{j\in\mathbf{A}_i} B_{i,j}\theta_j \tag{7}$$

where P_i is the power injection at bus i and θ_j is the voltage phasor angle at bus j, while $B_{i,j}$ is the imaginary part of the (i,j)-entry of the grid's admittance matrix. Let $P := (P_1, \cdots, P_N)^T \in \mathbb{R}^N$ be the power injection vector and $\theta := (\theta_1, \cdots, \theta_N) \in \mathbb{R}^N$ be the voltage phasor vector. Then (7) can be re-written as $P = B\theta$, where $B \in \mathbb{R}^{N\times N}$ is the susceptance matrix with the entries $B(i,i) = B_{i,i}$ and $B(i,j) = B_{i,j}$, if $j \in \mathbf{A}_i$, and 0 otherwise. Since, $P \sim \mathscr{N}(u_p, \Sigma_p)$, we have $\theta \sim \mathscr{N}\left(B^{-1}u_p, B^{-1}\Sigma_p\left(B^{-1}\right)^T\right)$, where $\mathscr{N}(\cdot)$ denotes a normal distribution. The measurement equation of a PMU installed at bus i is given by [42]

$$\begin{aligned} \chi_i &= \theta_i + v_i \\ \chi_{i,j} &= \theta_i - \theta_j + v_{i,j},\ i \in \mathbf{A}, j \in \mathbf{A}_i \end{aligned} \tag{8}$$

with $v_i \sim \mathscr{N}(0, r_i)$, and $v_{i,j} \sim \mathscr{N}(0, \rho_i)$ are the estimation uncertainties resulting from the perturbed grid conditions. The measurement vector $m_i := [\chi_1, \cdots, \chi_{i|\mathbf{A}_i}]^T$ is of dimension $D_i = \|\mathbf{A}_i\| + 1$. For brevity, (8) is written in the regression form as $m_i = H_i\theta + w_i$, where $H_i \in \mathbb{R}^{D_i\times N}$ is the associated regression matrix, $w_i := [v_i, v_{i1}, \cdots, v_{i|\mathbf{A}(i)|}]^T \sim \mathscr{N}(0, R_{w_i})$ with diagonal covariance. Let us define $R_{w(\mathbf{z})} = \text{diag}\left[R_{wi_j}\right]_{j=1,\cdots,R}$, $m(\mathbf{z}) = [m_{i_1}, \cdots, m_{i_R}]^T$, $w(\mathbf{z}) = [w_{i_1}, \cdots, w_{i_R}]^T$, and $\overline{H}(\mathbf{z}) = [H_{i_1}, \cdots, H_{i_R}]^T$. Thus, the multi-input multi-output PMU measurement equation is given as

$$m(\mathbf{z}) = \overline{H}(\mathbf{z})\theta + w(\mathbf{z}). \tag{9}$$

Using (9), we have $R_{m(\mathbf{z})}\theta = \overline{H}(\mathbf{z})R_\theta$, while $R_{m(\mathbf{z})} = \overline{H}(\mathbf{z})R_\theta\overline{H}(\mathbf{z})^T + R_{w(\mathbf{z})}$. Further, let us define $\theta|m(\mathbf{z})$ as a random variable θ conditioned on the random variable $m(\mathbf{z})$. Therefore, we have $\theta|m(\mathbf{z}) \sim \mathscr{N}(\hat{\theta}, R_e(\mathbf{z}))$.

Remark 6. *It is notable that the above analysis is different from the existing Kalman filter (KF)-based and allied formulation. KF only discusses process (estimation) noise, and not system perturbations. Therefore, although the analysis is on the similar lines, the optimized metric and the underlying process are different.*

Lemma 2. *The minimum mean squared error estimate of θ based on PMU output $m(\mathbf{z})$ given by $\hat{\theta}$ is $\hat{\theta} = \overline{\theta} +$*

$R_\theta H(\mathbf{z})^T (H(\mathbf{z}) R_\theta \overline{H}(\mathbf{z})^T + R_{w(\mathbf{z})})^{-1} (m(\mathbf{z}) - H(\mathbf{z})\bar{\theta})$ *with the covariance matrix given by*

$$R_e(\mathbf{z}) = \left(B^T \Sigma_P^{-1} B + \sum_{i \in \mathscr{N}} z_i H_i^T R_{w_i} H_i \right)^{-1}.$$

Proof. See Appendix B. □

Optimal PMU placement under perturbation must ensure grid estimation ability at the PDC. This is achieved by minimizing the mean squared error (MSE) given by $\mathbb{E}(\|\theta - \hat{\theta}\|^2)$. Therefore, an optimization problem is formulated as

$$(\mathbf{P}_2) : f(\mathbf{z}) = \min_{\mathbf{z}} J(\mathbf{z}) + \epsilon f_e(\mathbf{z}) \text{ s.t. } \mathbf{C}_1 \tag{10}$$

where ϵ is the estimation trade-off implying the importance of grid estimation using PMU data at the PDC, $f_e(\mathbf{z}) := \text{Trace}(R_e(\mathbf{z}))$, is a convex function by construction. The next lemma provides a continuous relaxation for the constraint $\mathbf{C}_1$.

Lemma 3. *For a polytope Poly($\mathscr{D}_R$), the discrete constraint $\mathbf{C}_1$ is equivalent to the continuous constraint $\mathbf{z} \in Poly(\mathscr{D}_R), \phi(\mathbf{z}) \geq R$ for $\phi(\mathbf{z}) := \sum_{i \in \mathscr{N}} z_i^\beta$ with $\beta > 1$.*

Proof. See Appendix C. □

Since, $\phi(\mathbf{z})$ is convex in $\mathbf{z}$, the constraint $\phi(\mathbf{z}) \geq R$ is a reverse convex constraint. As such, it is a difference of two convex sets, Poly($\mathscr{D}_R$) and $\{\mathbf{z} | \phi(\mathbf{z}) < R\}$. Also, as β decreases, $\phi(\mathbf{z})$ tends to a linear function. However, as $\beta \to 1$, the function $\phi(\mathbf{z}) - R$ approaches zero very quickly.

Proposition 1. *$\tilde{\phi}(\mathbf{z}) = \frac{1}{\phi(\mathbf{z})} - \frac{1}{R}$ can be used to measure the degree of satisfaction of the discrete constraint $\mathbf{C}_1$ in the sense that $\tilde{\phi}(\mathbf{z}) \geq 0 \ \forall \mathbf{z} \in Poly(\mathscr{D}_R)$ and $\tilde{\phi}(\mathbf{z}) = 0$ iff $\mathbf{z} \in \mathscr{D}_R$.*

Further, we define the mutual information between random variable θ and $m(\mathbf{z})$, $I(\theta; m(\mathbf{z})) = \mathscr{H}(\theta) - \mathscr{H}(\theta | m(\mathbf{z}))$ as

$$I(\theta; m(\mathbf{z})) = \frac{1}{2 \ln 2} \left(\ln |R_\theta| - \ln |R_e(\mathbf{z})| \right) \tag{11}$$

where $\mathscr{H}(\cdot)$ is the logarithmic entropy function leading to (11). This acts as a pointer to ambient grid estimation under perturbation at PDC. Relevant results using these parameters are given in Section IV.

It is notable that the expressions (7) and (8) are also based on the network equations, relating the dependence between multiple network parameters, leading to (9). Since all subsequent equations are mathematical manipulations of these representations, the appropriate lemmas and proofs ensure that the presented mathematics appropriately represents the system as described in Section II.

D. Solution to Optimal PMU Placement Problem

This subsection details the analysis of optimal solution to ($\mathbf{P}_2$) based on the mathematical simplifications in the previous subsection. Using Lemma 3 and Proposition 1 in ($\mathbf{P}_2$), we formulate a penalized optimization problem, which penalizes every non-zero instance of the relaxed constraint $\tilde{\phi}(\mathbf{z})$:

$$\min_{\mathbf{z}} F_\delta(\mathbf{z}) := f(\mathbf{z}) + \delta \tilde{\phi}(\mathbf{z}) \text{ s.t. } \mathbf{z} \in \text{Poly}(\mathscr{D}_R) \tag{12}$$

Algorithm 1: Penalty-aware Perturbation Robust Optimal PMU Placement Algorithm

1 : **Initialization**: Set $\kappa = 0$. Choose a feasible point $\mathbf{z}^{(0)} \in (0,1)^N$ for (10) using Algorithm 2
2 : Find δ s.t. $f(\mathbf{z}^{(0)})$ and $\left(\frac{1}{R} - \frac{1}{\phi(\mathbf{z}^{(0)})}\right)$ achieve equal significance.
3 : Set $\kappa \to \kappa + 1$.
4 : Solve (14) using Algorithm 2 to generate the next feasible point $\mathbf{z}^{(\kappa+1)}$.
5 : **Until** convergence.

Algorithm 2: Feasible Point Generation Algorithm

1 : Fetch generation counter $t = \kappa$
2 : **If** $t = 0$, create initial population of P vectors $\mathbf{P}^0 = \{\mathbf{z}_1^0, \mathbf{z}_2^0, \cdots, \mathbf{z}_P^0\} \subset \mathscr{D}_R$, s.t. $\|\mathbf{P}^t\| = P \ \forall t$
Otherwise, Use $\mathbf{P}^{t+1}$ generated in previous iteration
3 : Compute fitness value α_i^t of each vector in $\mathbf{P}^t$
4 : Choose $\mathbf{z}^{(\kappa)} \to \mathbf{z}_i^t$ having maximum α_i^t and set $t \to t+1$
5 : $p_0^t :=$ no. of vectors in $\mathbf{P}^t$ with $\alpha_i \geq \eta \alpha_{\max}$
6 : $\mathbf{V}_P^t :=$ set of those p_0^t vectors from $\mathbf{P}^t$
7 : Set $p_1^t = 2$, $p_2^t = 1$; generate crossover and mutation vectors using steps 8-9
8 : **Crossover vectors**: $\mathbf{V}_{CO}^t = C\left(\mathbf{V}_P^t, p_1^t\right)$
9 : **Mutation vectors**: $\mathbf{V}_M^t = M\left(\mathbf{V}_P^t, p_2^t\right)$
10 : Calculate fitness for these vectors, increment $p_1^t \to p_1^t + 1$ and $p_2^t \to p_2^t + 1$
11 : Repeat 8-11 till fitness for all new vectors $\geq \eta \alpha_{\max}$
12 : Choose best P vectors from these based on fitness
13 : **Update**: $\mathbf{P}^t \to \mathbf{P}^{t+1}$ using the selected P vectors.

where $\delta > 0$ is a penalty parameter. This penalized optimization problem is exact with a sufficiently large δ. It is notable that (12) is a minimization of a non-convex function over a convex set. However, by achieving the minimum for $F_\delta(\mathbf{z})$, an efficient PMU deployment strategy can be obtained under perturbed grid conditions with efficient grid estimation at the PDC. The pseudo-code for the proposed computational procedure used in finding the optimal solution to ($\mathbf{P}_2$) is given in Algorithms 1 and 2. However, as $\phi(\mathbf{z})$ is convex, we have

$$\begin{aligned} \phi(\mathbf{z}) \geq & \phi^{(\kappa)}(\mathbf{z}) = \phi(\mathbf{z}^{(\kappa)}) + \langle \nabla \phi(\mathbf{z}^{(\kappa)}), \mathbf{z} - \mathbf{z}^{(\kappa)} \rangle \\ = & -(\beta - 1) \sum_{i \in \mathscr{N}} (\mathbf{z}_i^{(\kappa)})^\beta + \beta \sum_{i \in \mathscr{N}} (\mathbf{z}_i^{(\kappa)})^{\beta - 1} \mathbf{z}_i \end{aligned} \tag{13}$$

where $\langle u, v \rangle$ denotes the inner product between the vectors u and v. Therefore, an approximate upper bound for $\frac{1}{\phi(\mathbf{z})}$ at $\mathbf{z}^{(\kappa)}$ can be obtained as $\frac{1}{\phi(\mathbf{z})} \leq \frac{1}{\phi^{(\kappa)}(\mathbf{z})}$ over the trust region $\phi^{(\kappa)}(\mathbf{z}) > 0$. Thus, at the κ-th iteration, following convex optimization needs to be solved to generate $\mathbf{z}^{(\kappa+1)}$

$$\begin{aligned} (\mathbf{P}_3) : \min_{\mathbf{z}} F_\delta^{(\kappa)}(\mathbf{z}) := & f(\mathbf{z}) + \delta \left(\frac{1}{\phi^{(\kappa)}(\mathbf{z})} - \frac{1}{R} \right) \\ & \text{s.t. } \mathbf{z} \in \text{Poly}(\mathscr{D}_R),\ \phi^{(\kappa)}(\mathbf{z}) > 0. \end{aligned} \tag{14}$$

($\mathbf{P}_3$) is solved using Algorithm 2 to generate the next feasible point. We compute the fitness of the i-th vector in $\mathbf{P}^t$ as the normalized value of $f(\mathbf{z})$ in ($\mathbf{P}_2$), given by $\alpha_i = \frac{f(\mathbf{z}_i^t)}{\sum_{i=1}^P f(\mathbf{z}_i^t)}$. After selecting the set of vectors $\mathbf{V}_P^t$ from $\mathbf{P}^t$, we pass them through the function $C(\cdot, \cdot)$ and $M(\cdot, \cdot)$ to generate crossover and mutation vectors, respectively. Partially matched crossover and simple inversion mutation are used respectively in crossover and mutation operations, owing to their capability

as a couple in achieving swift and best optimal solution [43].

To solve the optimization ($\mathbf{P}_3$), the approach in Algorithm 1 involves finding an appropriate penalty parameter δ that balances the original objective function $f(\mathbf{z})$ and the inverse of the convex function $\phi(\mathbf{z})$ (c.f. Lemma 3), thus integrating responsiveness to system conditions. Therefore, the optimization problem formulated for the κ-th iteration is as follows:

$$(\mathbf{P}_4):\ \delta^{(\kappa)} \rightarrow \arg\min_{\delta} \left| f(\mathbf{z}^{(\kappa)}) - \delta \left(\frac{1}{\phi^{(\kappa)}(\mathbf{z})} - \frac{1}{R} \right) \right|. \quad (15)$$

Subsequently, based on the above penalty parameter δ, Algorithm 2 generates new feasible points that approximate the solution to the overall optimization more accurately. To achieve this objective, following optimization problem is solved:

$$(\mathbf{P}_5):\ \mathbf{z}^{(\kappa+1)} \rightarrow \arg\min_{\mathbf{z}} \left\{ F_{\delta}^{(\kappa)}(\mathbf{z}) = f(\mathbf{z}) + \delta^{(\kappa)} \left(\frac{1}{\phi^{(\kappa)}(\mathbf{z})} - \frac{1}{R} \right) \right\}$$
$$\text{s.t. } \mathbf{z} \in \text{Poly}(\mathscr{D}_R),\ \phi^{(\kappa)}(\mathbf{z}) > 0.$$

We start with an initial guess $\mathbf{z}^{(0)}$ and use Algorithm 2 to solve the optimization problem ($\mathbf{P}_5$). Then, for each iteration κ, we use above-generated outcome $\mathbf{z}^{(\kappa)}$ to solve the optimization in ($\mathbf{P}_4$) and adjust $\delta^{(\kappa)}$. Next, with the updated $\delta^{(\kappa)}$, we resolve the optimization ($\mathbf{P}_5$) to obtain the next feasible point $\mathbf{z}^{(\kappa+1)}$. This process is repeated until the changes in $\mathbf{z}$ and δ meet the plateau convergence criteria, i.e., do not exhibit any further change. In this work, $\eta = 0.9$ is utilized in generating the successive feasible points using Algorithm 2.

Remark 7. *Please note that, Algorithm 2 starts with a binary decision variable* $\mathbf{z}$*, i.e.,* $\mathbf{z}^{(0)}$*. Consequently, the subsequent vectors generated using selection, crossover, and mutation are all binary, ensuring a final solution in the* 0/1 *structure.*

Remark 8. *It is worth highlighting here that, Algorithm 2 can be modified as per the convenience of the implementer. Since the PMU placement optimization is a planning problem (making the run time inconsequential) the key metrics defining the choice of any such algorithmic framework are, the assurance of convergence to a binary vector and processor space complexity, i.e., the available storage on the device. Further, in case one could opt for a system with a decent storage capacity, the constraint on space complexity can be relaxed.*

E. Convergence and Complexity Analysis of the Algorithms

Proof of convergence: For Algorithm 1, with the simplifications from the previous subsection, the algorithm starts with an initial feasible solution $\mathbf{z}^{(0)}$ and an initial penalty parameter δ, at iteration $\kappa = 0$. At each iteration, δ ensures that constraint violations are increasingly penalized to discourage sub-optimal solutions. The penalized objective function at iteration κ is defined as $F_{\delta}^{(\kappa)}(\mathbf{z}^{(\kappa)})$. It is notable that $F_{\delta}(\mathbf{z}) \leq F_{\delta}^{(\kappa)}(\mathbf{z})$ $\forall \mathbf{z}$, and $F_{\delta}(\mathbf{z}^{(\kappa)}) = F_{\delta}^{(\kappa)}(\mathbf{z}^{(\kappa)})$. Also, since $\mathbf{z}^{(\kappa+1)}$ and $\mathbf{z}^{(\kappa)}$ are respectively the optimal solution and a feasible point for (14), we have $F_{\delta}^{(\kappa)}(\mathbf{z}^{(\kappa+1)}) < F_{\delta}^{(\kappa)}(\mathbf{z}^{(\kappa)})$. Therefore, $F_{\delta}(\mathbf{z}^{(\kappa+1)}) \leq F_{\delta}^{(\kappa)}(\mathbf{z}^{(\kappa+1)}) < F_{\delta}^{(\kappa)}(\mathbf{z}^{(\kappa)}) = F_{\delta}(\mathbf{z}^{(\kappa)})$, i.e., $\mathbf{z}^{(\kappa+1)}$ is a better feasible point than $\mathbf{z}^{(\kappa)}$ for (12), which proves the efficacy of Algorithm 2. Further, for sufficiently large $\delta > 0$, $\tilde{\phi}(\mathbf{z}^{(\kappa)}) \rightarrow 0$, yielding an optimal solution of the binary non-linear optimization in (10).

Since the convergence and optimality of Algorithm 1 depends on the convergence and the generation of the subsequent feasible point by the embedded algorithm, i.e., Algorithm 2. For Algorithm 2, genetic operations such as, selection, crossover, and mutation, preserve and potentially improve fitness, with mechanisms like elitism ensuring that the best solutions are carried forward. Starting with a diverse population, the algorithm evaluates the fitness of each individual instance of $\mathbf{z}$ based on the function α_i^t. A subset of the population is then selected for reproduction based on fitness, favoring individuals with better fitness scores. Genetic operations are applied to produce a new generation, designed to explore the solution space while preserving high-quality solutions. In the process, elitism and diversity maintenance prevent premature convergence [44]. Under these conditions, assuming sufficient population size and generations, which is the case in NP-hard problems, the algorithm is guaranteed to converge in probability to the global optimum of the fitness function, with a near unity MI and sufficiently reduced MMSE.

Remark 9. *The zeroth generation's population* $\mathbf{P}^0$ *generated in Algorithm 2 should preferably encompass diversity, for the future estimates to converge quickly towards optimality. The diversity within vectors in* $\mathbf{P}^0$ *could simply be ensured by measuring Hamming distance between them.*

Complexity of the Algorithms: It is notable that the initialization step of Algorithm 1 possesses $\mathscr{O}(1)$ complexity. Since the choice of the penalty parameter is done step-wise, the rest of the steps involve no floating point operations per second. Next, for Algorithm 2, if each solution's feasibility check involves evaluating $f(\mathbf{z})$, and if there are P such solutions, the resultant complexity is $\mathscr{O}(P) \times \mathscr{C}_{f(\mathbf{z})}$, where $\mathscr{C}_{f(\mathbf{z})}$ denotes the complexity of evaluating $f(\mathbf{z})$. Finally, if Algorithm 2 runs for G generations, the total complexity $\mathscr{C}$ is

$$\mathscr{C} = \mathscr{O}(1) + GP \times \mathscr{C}_{f(\mathbf{z})} \approx GP \times \mathscr{C}_{f(\mathbf{z})}. \quad (16)$$

Next, we evaluate the complexity of operating $f(\mathbf{z})$. Since in the evaluation of $f(\mathbf{z}) = \min_{\mathbf{z}} J(\mathbf{z}) + \epsilon f_e(\mathbf{z})$, matrix inversion, summation, and multiplication operations are involved, the total algebraic complexity is $\mathscr{O}(N^3) + \mathscr{O}(N + \|\mathbf{z}\|)$, where $\|\mathbf{z}\|$ represents the cardinality operation on the PMU placement vector $\mathbf{z}$. Thus, the total complexity is written as:

$$\mathscr{C}_{f(\mathbf{z})} = \mathscr{O}(N^3) + \mathscr{O}(N + \|\mathbf{z}\|) + \mathscr{O}(\text{optimization}) \quad (17)$$

where $\mathscr{O}(\text{optimization})$ is the complexity involved in the optimization aiming at reducing the search space of 2^N feasible vectors using the genetic search approach in Algorithm 2. If we assume a heuristic method where each iteration involves evaluating $f(\mathbf{z})$ for P candidates and runs for G generations, the complexity of optimization could be represented as $O(G \times P \times N^3)$, leading to a total complexity of

$$\begin{aligned}\mathscr{C}_{f(\mathbf{z})} =& \mathscr{O}(N^3) + \mathscr{O}(N + \|\mathbf{z}\|) + O(G \times P \times N^3) \\ =& \mathscr{O}(N + \|\mathbf{z}\|) + O((1 + G \times P) \times N^3).\end{aligned}$$

TABLE I: IEEE standard transmission networks specifications.

Test system	Loc. of ZIB	Loc. of radial buses
IEEE 14-bus	7	8
IEEE 30-bus	6, 9, 22, 25, 27, 28	1, 13, 26
IEEE 57-bus	4, 7, 11, 21, 22, 24, 26, 34, 36, 37, 39, 40, 45, 46, 48	33
IEEE 118-bus	5, 9, 30, 37, 38, 63, 64, 68, 71, 81	10, 73, 87, 111, 112, 116, 117

TABLE II: Optimal hyper-parameter settings and convergence details of Algorithm 1; c.t.: convergence time.

Test system	ϵ	δ	c.t. (s) ($\lambda = 1$)	c.t. (s) ($\lambda = 0$)
IEEE 6-bus	0.27	0.09	43.12	43.37
IEEE 14-bus	0.36	0.10	62.94	60.77
IEEE 30-bus	0.57	0.10	79.14	76.53
IEEE 57-bus	1.00	1.00	80.47	80.37
IEEE 118-bus	1.20	1.00	216.31	216.19

Therefore, the overall algorithmic complexity is as follows:

$$\begin{aligned}\mathscr{C} =& GP\left[\mathscr{O}(N+\|\mathbf{z}\|)+O((1+G\times P)\times N^3)\right]\\ =& \mathscr{O}\left(\left\{N+\|\mathbf{z}\|+[1+GP]\,N^3\right\}GP\right).\end{aligned} \tag{18}$$

Based on the above analysis, the convergence time is mentioned in Table II, while the rest of the PMU placement and allied results are presented in the next section.

IV. Results and Discussion

The proposed grid controllability aware practical PMU deployment strategy was tested on standard IEEE test systems without as well as with considering perturbations. The impact of ZIB was considered to see the variation of perturbation on different grid topologies. No direct redundancy was offered to any node by setting $\sigma_i = 1$, $\forall i$.

The proposed optimal PMU placement strategy is compared with the conventional approaches with sufficient input current channels, as in [7], [10], and with limited input current channels, as in [16], [17], [26]. Further, for completeness of analysis considering all extreme power grid situations, we test the effectiveness of the proposed controllability-aware optimal deployment of PMUs with limited input current channels using $\%$ observability, $\%$ controllability, numerical redundancy, and redundancy overhead metrics in single PMU loss (SPL) and single line loss (SLL) conditions. Such conditions do not represent the loss of one out of the three phases, rather a loss of all phases. Therefore, such events do not lead to any grid asymmetry. Further, the situations arising from any grid asymmetry is accurately monitored by the estimation algorithms embedded in the state-of-the-art PMUs [45].

The results are verified for IEEE 6, 14, 30, 57, and 118-bus systems. The network specifications are given in Table I. Algorithm 1 was implemented on E3-1285 v6 CPU (@4.10 GHz); the optimal hyper-parameters are listed in Table II. During simulation, $\beta = 1.45$ was found for fastest convergence.

Remark 10. *It is observed that the convergence rate for Algorithm 1 is almost same irrespective of the choice of controllability or observability based PMU deployment strategy, as shown using c.t. in Table II. Thus, from an algorithmic viewpoint, no significant performance reduction occurs.*

TABLE III: Optimal PMU placement in perturbed IEEE 6-bus system; Conv.: conventional, Rev.: revised, CC: current channels

No. of CC per PMU (rev.)	Conv. opt. PMU placement (suff. CC)	Rev. opt. PMU placement
1	4, 5	1, 3, 5
2	4, 5	3, 6
3	4, 5	4, 5

A. Test Case: Demonstration of Optimal Placement of PMUs with Limited Input Current Channels in IEEE 6-Bus System

For an IEEE 6-bus system, by setting $\lambda = 0$ we get the optimal PMU placement considering grid observability only, as given in Table III. However, when a perturbed system is considered, line observability gains significance over node-based grid observability. From the updated solution using (12), the optimum PMU placement changes, both in number and locations. This proves that the conventional placement strategy is insufficient to monitor actual power grids, considering its perturbations. In contrast, with the notion of controllability-aware PMU placement strategy as proposed in this paper, it is able to provide better line observability with increased grid observability index, as observed from Fig. 4(b).

From Table III we infer that, for a perturbed system the optimal PMU deployment locations and the number of PMUs depend on the number of input current channels in a PMU. Typically the number of input current channels is considered unlimited thus far in literature. In the simulations, it was noted that, for a 6-bus system optimum controllability is attained when PMUs are installed at bus $\{2, 4, 6\}$, with 1 input current channel per PMU, while the vector updates to $\{3, 6\}$ considering 2 input current channels. However, as the number of input current channels per PMU reach 3, the maximum node incidence order equals the input current channels available per PMU. In such a case, the optimal PMU placement vector reorients to $\{4, 5\}$, which is the same as that rendered by the conventional placement strategy, owing to fulfilling the sufficiency assumption on the input current channels per PMU. These results demonstrate that optimal PMU placement vector changes with limited number of input current channels per PMU, which is the case in practical PMUs.

The incidence matrix for the 6-bus system is given as [46]

$$\mathbf{A}_6 = \begin{bmatrix} 1 & 0 & 1 & 0 & 0 & 0 \\ 0 & 1 & 0 & 0 & 0 & 0 \\ 0 & 1 & 1 & 0 & 0 & 0 \\ 1 & 0 & 0 & 1 & 0 & 0 \\ 1 & 0 & 0 & 0 & 1 & 0 \\ 1 & 0 & 0 & 0 & 0 & 1 \end{bmatrix}. \tag{20}$$

Again, based on the data in [32], we have $\mathbf{A}_{l,6} = [\mu_{i,j}]_{i,j\in\{1,\cdots,6\}}$, as given in (19).We use this data to find $\mathbf{O} = [o_1, \cdots, o_6]$, where the i-th vector entry is given by $o_i = \sum_{j\in\mathbf{A}_i} \mu_{i,j}$. Here, the summation over j is evaluated on the node incidence vector of node i, defined as $\mathbf{A}_i$ in Section II. With these definitions, our proposed Algorithms 1 and 2 are used to find the optimum PMU placement in the IEEE 6-bus system, considering the deployment of PMUs with 1 input current channel, i.e. $l_i = 1$, $\forall i \in \{1, \cdots, 6\}$, as mentioned in Table III. Using the optimal PMU placement result, Table IV

$$\mathbf{c}_6=\begin{bmatrix}0 & 0.1064 & 0 & 0.0532 & 0.0851 & 0\\ 0 & 0 & 0.0532 & 0.0532 & 0.1064 & 0.0745\\ 0 & 0 & 0 & 0 & 0.1277 & 0.0213\\ 0 & 0 & 0 & 0 & 0.2128 & 0\\ 0 & 0 & 0 & 0 & 0 & 0.1064\\ 0 & 0 & 0 & 0 & 0 & 0\end{bmatrix}; \mathbf{A}_{l,6}=\mathbf{c}_6\odot\begin{bmatrix}2z_1 & 0 & z_1+z_3 & 0 & 0 & 0\\ 0 & 2z_2 & 0 & 0 & 0 & 0\\ 0 & z_3+z_2 & 2z_3 & 0 & 0 & 0\\ z_4+z_1 & 0 & 0 & 2z_4 & 0 & 0\\ z_5+z_1 & 0 & 0 & 0 & 2z_5 & 0\\ z_6+z_1 & 0 & 0 & 0 & 0 & 2z_6\end{bmatrix} \quad (19)$$

TABLE IV: Demonstration of controllability-aware optimal PMU placement on IEEE 6-bus system, at base MVA = 100.

Bus	True voltage (p.u.)	Estimated bus voltage (p.u.)			Estimation error (%)		
		Normal	SPL	SLL	Normal	SPL	SLL
1	1.05	1.0497	1.0492	1.0496	0.0286	0.0762	0.0381
2	1.05	1.0495	1.0492	1.0494	0.0476	0.0762	0.0571
3	1.07	1.0694	1.0693	1.0694	0.0561	0.0654	0.0561
4	1.02	1.0193	1.0189	1.0191	0.0686	0.1078	0.0882
5	1.002	1.0019	1.0018	1.0019	0.01	0.02	0.01
6	0.982	0.9814	0.9812	0.9813	0.0611	0.0815	0.0713

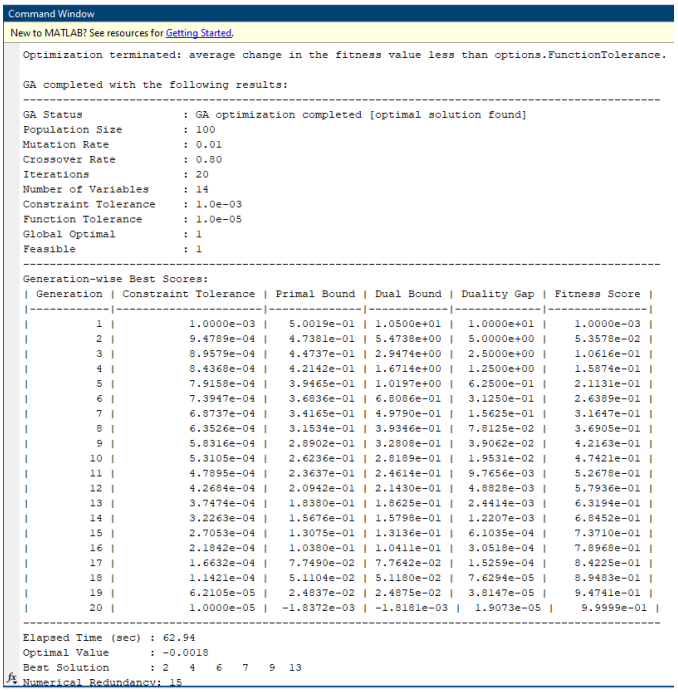

Fig. 3: MATLAB output log file of optimal PMU location in IEEE 14-bus system.

demonstrates the ability of the proposed controllability-aware optimal placement of PMUs in reconstruction of the complete grid network in a standard IEEE 6-bus test system. From Table IV we note that error in the estimated value of the node voltage is very small ($\leq 10^{-3}$), which is explained further in Section IV-D from an information theoretic perspective, for various generic grid systems. We further observe that this estimation is equally robust under grid adversities, such as SPL and SLL.

B. Variation of Optimal Placement Policy with PMU's Input Current Channel Limitations in Perturbed Power Networks

Table V shows the optimal PMU placement for standard IEEE test systems suggested by the proposed strategy under normal and perturbed grid conditions while neglecting the presence of ZIBs. It can be seen that, with the proposed perturbation-robust optimal PMU deployment, the location as well as the number of minimum required PMUs change. Further, contrasting the proposed controllability-aware optimal PMU placement solution with the optimal placement of PMUs with 1 input current channel, it can be noted that the proposed strategy is able to achieve optimum grid observability and controllability at a lesser number of PMUs, placed strategically at different nodes. This reduction in the optimal PMU number results from harnessing spatial correlation in PMU data during grid reconstruction and estimation at PDC, as given by (9). Therefore, since the final PMU placement optimization is sensitive to robust grid estimation at the data collector, the optimal placement strategy obtained in this paper not only ensures grid observability, but also takes into consideration the correlation among the various grid nodes. Consequently, the optimal placement changes in terms of the optimal number of PMUs and the nodes where they are to be deployed. Naturally, grids showing higher correlation of parameters among its constituent nodes can ensure optimal system controllability (which ensures numerical observability by definition) even at a reduced number of PMUs, such as in IEEE 14-bus network.

Table VI shows the change in optimal PMU deployment considering a perturbed grid in the presence of ZIBs. It was observed that the number of PMUs for optimal grid monitoring drop in this case. However, the optimal deployment vector still differs from the conventional placement scenario. Again, comparing the proposed PMU placement with the conventional deployment of single channel PMUs, it can be inferred that the proposed PMU deployment vector provides superior deployment strategy with reduced number of PMUs and robust grid monitoring under perturbations.

Further, for verifying the convergence, solution time, numerical redundancy, and the optimal solution, we present the output log file generated by MATLAB (for brevity, we only present for the IEEE 14-bus system). From Fig. 3, we note that, in case of the IEEE 14-bus system, the constraint violation is ensured below a sufficiently small threshold in every generation of the proposed solution algorithm. The convergence can be noted by the continuously decreasing duality gap and almost negligible change in the fitness score, which has been used as a stopping criterion (note the 'optimization terminated' line in the figure). Furthermore, the 'best solution' generated by the algorithm can be noted to match the one in the first row of Table V, within the run-time mentioned in Table II, and the numerical redundancy mentioned in Table X for controllability-aware optimal PMU deployment in the IEEE 14-bus system.

Next subsections establish this fact in further details using MMSE, mutual information, and contingency analysis for various deployment scenarios.

TABLE V: Controllability-aware optimal PMU placement (OPP) for different IEEE test systems under perturbation without considering ZIB

Test system	Conventional OPP ($\lambda = 0$)		Controllability-aware OPP ($\lambda = 1$)
	Sufficient current channels [7], [10]	1 current channel [16], [17], [26]	(1 current channel)
14-bus	2, 6, 7, 9	1, 3, 4, 6, 9, 11, 12, 14	2, 4, 6, 7, 9, 13
30-bus	1, 7, 8, 10, 11, 12, 18, 23, 26, 30	1, 2, 4, 5, 6, 10, 12, 13, 15, 16, 18, 19, 24, 27, 29	1, 5, 6, 9, 10, 12, 17, 19, 22, 24, 25, 27, 29
57-bus	2, 6, 10, 12, 19, 22, 25, 27, 32, 36, 41, 45, 46, 49, 52, 55, 57	1, 3, 5, 6, 9, 11, 12, 14, 15, 17, 19, 20, 21, 24, 25, 28, 29, 30, 32, 35, 38, 41, 43, 45, 49, 50, 51, 53, 54, 56	1, 2, 4, 6, 9, 12, 15, 19, 20, 22, 24, 26, 29, 30, 31, 32, 35, 36, 41, 45, 46, 50, 51, 53, 54, 56, 57
118-bus	2, 5, 9, 11, 12, 17, 21, 24, 25, 28, 34, 37, 40, 45, 49, 52, 56, 62, 63, 68, 73, 75, 77, 80, 85, 86, 90, 94, 101, 105, 110, 114	1, 3, 6, 8, 10, 11, 12, 15, 17, 19, 20, 21, 23, 27, 28, 29, 32, 34, 35, 40, 41, 43, 45, 46, 49, 50, 51, 52, 54, 56, 60, 62, 65, 66, 70, 72, 75, 76, 77, 78, 80, 83, 85, 86, 87, 89, 90, 92, 94, 96, 100, 101, 105, 106, 108, 110, 111, 112, 114, 117	1, 2, 5, 9, 10, 11, 12, 15, 17, 21, 22, 25, 26, 28, 29, 34, 35, 37, 40, 45, 46, 49, 52, 53, 56, 62, 63, 68, 72, 75, 76, 77, 80, 84, 85, 87, 89, 92, 94, 96, 100, 105, 107, 110, 114

TABLE VI: Controllability-aware OPP for different IEEE test systems under perturbation considering ZIB

Test system	Conventional OPP ($\lambda = 0$)		Controllability-aware OPP ($\lambda = 1$)
	Sufficient current channels [7], [10]	1 current channel [16], [17], [26]	(1 current channel)
14-bus	2, 6, 9	1, 4, 9, 11, 13	2, 4, 6, 9, 13
30-bus	2, 4, 12, 17, 19, 24	1, 3, 5, 9, 11, 12, 17, 19, 23, 24, 29	1, 2, 4, 6, 7, 12, 17, 19, 24
57-bus	1, 6, 9, 19, 29, 30, 32, 38, 51, 54, 56	1, 3, 6, 9, 12, 15, 19, 20, 25, 28, 29, 30, 32, 35, 38, 41, 49, 50, 51, 53, 54, 56	1, 3, 5, 9, 12, 15, 19, 20, 25, 29, 31, 32, 42, 49, 50, 51, 53, 54, 56
118-bus	2, 11, 12, 17, 21, 23, 28, 34, 40, 45, 49, 52, 56, 62, 71, 75, 77, 80, 85, 87, 90, 94, 102, 105, 110, 115	1, 3, 6, 11, 12, 15, 17, 19, 21, 22, 24, 26, 27, 29, 31, 32, 34, 36, 40, 42, 43, 45, 46, 49, 50, 51, 52, 54, 56, 59, 62, 66, 70, 75, 76, 77, 79, 80, 83, 85, 86, 89, 90, 92, 94, 96, 100, 101, 105, 107, 109, 110, 114	1, 2, 6, 11, 12, 17, 21, 23, 27, 28, 32, 34, 36, 40, 42, 45, 46, 49, 53, 56, 62, 71, 75, 76, 77, 79, 80, 84, 85, 87, 89, 90, 92, 94, 96, 100, 102, 105, 107, 109, 110, 115

Remark 11. *It is notable that, the objective of our analysis is different as compared to the state-of-the-art PMU placement approach which consider single current channel or multiple current channel PMUs. Our PMU placement strategy aims to jointly optimize PMU cost, wideband system monitoring through line observability reward and node weight, MI, MMSE, and grid estimation at PDC. As a consequence, it provides clear advantage over the methods proposed in literature [19], [23], which do not jointly address all these system performance parameters in their optimization goals.*

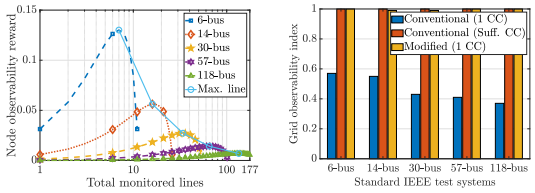

(a) (b)

Fig. 4: (*a*) Normalized node observability versus total monitored lines, (*b*) aggregate grid observability for different IEEE test systems.

C. Variation of Grid Observability with Controllability-Aware Optimal PMU Placement

Fig. 4(*a*) shows the variation of normalized node observability reward defined as $\xi_i = \frac{\sum_{j\in\mathbf{A}_i}\mu_{i,j}}{\sum_{i=1}^{N}\sum_{j\in\mathbf{A}_i}\mu_{i,j}}$ for various IEEE standard test systems, with the total lines monitored in the grid. It provides a very important observation with the number of lines being monitored by the PMUs. It has been considered thus far in literature that all PMUs have sufficient current cards to monitor all incident lines to the nodes on which they are installed. However, with the increase in grid size, such an assumption is not practical. It can be seen from Fig. 4(*a*) that an optimum normalized node observability reward can be attained with a limited number of direct monitored lines, which translates to limited current cards per PMU. As we try to monitor more than optimal number of lines, the cost of installation increases, thus resulting in a decrease in the reward against observing a node. Thus, a revised PMU placement vector with limited current cards is proposed in the previous subsection. This also highlights the assumption insufficiency in the conventional deployment strategy.

Fig. 4(*b*) shows the aggregate grid observability index $\boldsymbol{\omega}^T c \odot A \odot \left(\mathbf{z}^T\mathbf{S}^T\mathbb{1} + \mathbf{I}\mathbf{S}\mathbf{z}\right)\boldsymbol{\omega}$ for different IEEE standard test systems, and contrasts the different optimal PMU deployment scenario. It can be observed that, for conventional PMU deployment, as achieved with $\lambda = 0$ in this work, a normalized aggregate grid observability index of unity is achieved for all grid sizes. It can also be observed that as the assumption is relaxed to achieve the practical device constraint, we observe a significant drop in the grid observability index. This, results in an inefficient grid estimation at the PDC under perturbed system state, as detailed in the next subsection. However, it can be noted that, for the proposed controllability-aware optimal PMU deployment, a normalized grid observability index tending to unity is achieved for all standard grid topologies.

D. MMSE and Mutual Information for Controllability-Aware Optimal PMU Placement

Table VII shows the comparison of MMSE and mutual information between the conventional deployment and the proposed controllability-aware optimal PMU deployment for different IEEE test systems. It can be observed that MMSE decreases with the proposed controllability-aware deployment, implying a robust grid reconstruction at the PDC using the data from optimally deployed PMUs with single input current channel in perturbed network conditions. Further, the

TABLE VII: Comparison of MMSE and mutual information (MI) for conventional versus controllability-aware optimal PMU deployment ignoring ZIB; syst.: system

Test syst.	Conventional		Controllability-aware	
	MMSE	Normalized MI (bit)	MMSE	Normalized MI (bit)
14-bus	1.0123	0.1	3×10^{-3}	1
30-bus	1.0155	0.2	2.9×10^{-3}	1
57-bus	1.0193	0.6	2.5×10^{-3}	1
118-bus	1.0605	0.6	2.7×10^{-3}	1

TABLE VIII: Comparison of MMSE and MI for conventional versus controllability-aware optimal PMU deployment considering ZIB

Test syst.	Conventional		Controllability-aware	
	MMSE	Normalized MI (bit)	MMSE	Normalized MI (bit)
14-bus	1.0216	0.1	4.7×10^{-3}	0.96
30-bus	1.0127	0.1	4.9×10^{-3}	0.96
57-bus	1.0181	0.52	4.3×10^{-3}	0.99
118-bus	1.07	0.5	4.4×10^{-3}	1

MI $I(\theta, z(\mathbf{x}))$ is very less for the conventional deployment strategy; thus, for a perturbed grid, mutual information content at the direct monitored nodes about the pseudo-monitored nodes is inadequate. In contrast, the controllability-aware optimization formulation achieves the mutual information to unity for the estimation of direct and pseudo-monitored nodes in perturbed power networks. This ensures proper grid estimation at the PDC under any perturbation state, thus ensuring controllability as defined in the scope of this paper.

Table VIII shows a similar comparison between the two deployment scenarios while considering the presence of ZIBs. It can be seen that under conventional PMU deployment, MMSE increases while mutual information decreases further, owing to a drop in PMU numbers. However, with the proposed PMU deployment, grid estimation at the PDC using PMU data becomes robust with a decrease in MMSE while the mutual information tends to unity, even with the consideration of ZIB.

Remark 12. *Marginal drop in MI observed while considering the presence of ZIB can be attributed to the lesser requirement of PMUs to achieve the same MMSE as before, while the value of the correlation between the grid nodes drops at the PDC.*

E. Performance of Controllabilty-Aware Optimal PMU Placement under Grid Perturbations

This subsection presents the robustness of the proposed optimal PMU placement strategy under various grid adversities. The key performance indices used in this work are defined as follows: 1) Observability (Obs.) is defined as the percentage of grid nodes connected directly to a PMU or at a distance of 1-hop from a node having PMU; 2) Controllability (Control.) is defined as percentage of nodes correctly estimated within a tolerable error threshold using the PMU data at the data collector; 3) Grid controllability cost (GCC) is defined as the ratio of total installation cost to the per unit grid controllability. Cost of installing a PMU is proportional to the number of input current channels in the device.

From Tables VII and VIII, we have already established that the MMSE and mutual information provided by the conventional PMU deployment policy is unsatisfactory when compared to the proposed controllability-aware PMU placement. This metric directly translates to an inferior observability and controllability using the data from PMUs under conventional deployment strategy in perturbed power networks. Following this observation, we detail the aspects of grid adversities, such as line loss and PMU loss in Table IX. It is worth noting that, the optimization ($\mathbf{P}_3$) is different from the ones noted in references [19] and [23]. The key difference lies in the mathematical structure as well as the logical design of the involved objective function. ($\mathbf{P}_3$) focuses on optimal grid observability while ensuring a minimized (bounded) attribute estimation error for all the nodes, especially the pseudo-monitored nodes, using the data from the optimally placed single current channel PMUs in the perturbed power network. Since the objective function is logically as well as structurally different from the formulations in the state-of-the-art, the obtained results in terms of the number of PMUs and their locations are different from the ones that are achieved in the conventional optimal PMU placement literature.

From Table IX we observe that, in conventional optimal placement ($\lambda = 0$) for PMUs with sufficient input channels, SPL or SLL leads to a drop in observability as well as controllability, owing to the loss in the number of observed nodes, which then manifests to an erroneous estimation of grid nodes at the PDC. For the realistic deployment case, considering PMUs with 1 input current channel, we note that the drop in observability and controllability under SPL and SLL is severer. Contrasting the GCC values in both these cases, it is inferred that though an increased observability and controllability is achieved considering a hypothetical case of PMUs with sufficient input channels, the corresponding cost is also higher. Furthermore, this cost increases with the grid size. Considering the impact of ZIB, the number of PMUs that need to be deployed decreases. This directly translates to a reduced grid observability and controllability under SPL and SLL. Also, as the number of PMUs and total grid controllability has dropped simultaneously, a similar GCC is noted.

From the contingency analysis for controllability-aware PMU deployment ($\lambda = 1$) we observe that, as a result of the proposed PDC-end estimation approach with optimized MI and MMSE values, the proposed strategy renders superior performance under grid adversities resulting from SPL and SLL. Further, from the GCC values we note that, the controllability cost is substantially lower than the GCC in case of conventional optimal PMU deployment. A similar inference can be drawn for the case when ZIB is considered. *For the case of IEEE* 118*-bus system, considering SPL, we achieve a gain of* $\approx 19\%$ *(for PMUs with sufficient input channel) and* $\approx 49\%$ *(for PMUs with* 1 *input channel) using the proposed controllability-aware PMU placement policy. Similarly, under SLL, these values change to* $\approx 16\%$ *and* $\approx 43\%$*, respectively. Furthermore,* $\approx 77\%$ *and* $\approx 76\%$ *decrease in GCC is noted for SPL and SLL adversities, respectively.*

Remark 13. *The optimality of the solutions obtained for the PMU placement optimization in* (3) *can be noted using the high MI (*≈ 1*, i.e., close to saturation) and reduced MMSE,*

TABLE IX: Comparison of conventional OPP and controllability-aware OPP under various grid adversities

	Bus syst.	Conventional OPP ($\lambda = 0$)												Controllability-aware OPP ($\lambda = 1$) (1 current channel)					
		Sufficient current channels [7], [10]						1 current channel [16], [17], [26]											
		Obs. (%)		Control. (%)		GCC		Obs. (%)		Control. (%)		GCC		Obs. (%)		Control. (%)		GCC	
		SPL	SLL	SPL	SLL	SPL	SLL	SPL	SLL	SPL	SLL	SPL	SLL	SPL	SLL	SPL	SLL	SPL	SLL
No ZIB	14	71.12	78.87	53.12	57	32	29.82	45	50.22	33.33	35	24	22.88	100	100	100	100	8	8
	30	75.47	79.11	55	57.13	56.36	54.26	46.16	53.12	37.16	40	40.36	37.5	100	100	100	100	15	15
	57	77.63	81.14	56.17	58.5	85.45	82.05	49.32	54.04	44	47.9	68.18	62.63	100	100	100	100	30	30
	118	81.19	84.01	60	63.47	260	245.79	51.11	57	45.12	50.02	132.98	119.95	100	100	100	100	60	60
ZIB	14	66.67	69.12	47.34	51.01	31.69	29.41	40.01	45.8	32.13	34.15	15.56	14.64	98.96	99.73	100	100	5	5
	30	67.76	68.33	49.11	53.4	50.91	46.82	41	47.16	36.5	38.25	30.14	28.76	98.73	99.51	100	100	11	11
	57	71.32	73.73	50.07	55.12	65.91	59.87	43	50	39.01	41	56.4	53.66	99	100	100	100	22	22
	118	75.32	77.89	53.63	56.66	259.18	245.32	47.77	53.07	43.12	47.77	122.91	110.95	100	100	100	100	53	53

TABLE X: Numerical observability in controllability-aware optimal PMU placement solution

Test bus syst.	Neglecting ZIB									Considering ZIB								
	Numerical redundancy			Redundancy overhead			Numerical observability (Y/N)			Numerical redundancy			Redundancy overhead			Numerical observability (Y/N)		
	Normal	SPL	SLL	Normal	SPL	SLL	Normal	SPL	SLL	Normal	SPL	SLL	Normal	SPL	SLL	Normal	SPL	SLL
14	15	14.571	14.833	1	0.571	0.833	Y	Y	Y	15	14.571	14.833	1	0.571	0.833	Y	Y	Y
30	37	34.692	36.373	7	4.692	6.373	Y	Y	Y	42	39.5	41.288	12	9.5	11.288	Y	Y	Y
57	82	79.519	81.274	25	22.519	24.274	Y	Y	Y	85	82.912	84.284	28	25.912	27.284	Y	Y	Y
118	162	158.956	161.314	44	40.956	43.314	Y	Y	Y	168	165.255	167.288	50	47.255	49.288	Y	Y	Y

as presented in Tables VII and VIII. Further assurance on the optimality of the presented solutions can be gained from the bounded estimation error for the node voltage of IEEE 6*-bus system mentioned in Table IV.*

Remark 14. *Validity of the mathematics behind Algorithms 1 and 2 follow from the finite-time convergence results shown in Table II of the manuscript. Furthermore, the optimality of these algorithms is observed through the solution achieved for the proposed formulations ($\mathbf{F}_1$) and ($\mathbf{F}_2$), tabulated in Tables V and VI. The optimality is demonstrated through substantially reduced MMSE, near-unity mutual information, and near-unity grid observability rewards achieved through the solutions, and presented in Tables VII, VIII, and Fig. 4(b).*

F. Numerical Observability in Controllability-Aware Optimal PMU Placement

Numerical observability ensures the ability of estimating the entire grid at the PDC using optimal PMU placement positions [47]. This aspect of analysis is detailed from an information theoretic viewpoint in Tables VII and VIII, using MMSE and MI metrics for different standard IEEE test systems and considering the presence as well of absence of ZIBs. This subsection aims to relook at this aspect from redundancy view point. To this end, we define redundancy overhead to quantify observability in the proposed controllability-aware optimal PMU placement strategy. Numerical redundancy quantifies the total measurement redundancy achieved using a given PMU placement solution. This is a baseline measure, which is a necessary condition for guaranteeing a bounded state estimation for all grid nodes at the PDC. To suffice this necessity, the value of measurement redundancy must be more than the total number of nodes in the power network. It is notable that, non-information theoretic measure can never make for a sufficient condition for bounded estimation. As a result, in this work, beyond ensuring measurement redundancy, we aim to maximize MI and minimize MMSE as a joint objective in our PMU placement optimization in (12).

Numerical redundancy for an N-node grid is defined as $\gamma = \mathbf{z}^T\mathbf{A}^T\mathbf{A}\mathbf{z}$. Further, numerical observability under SLL is defined as $\gamma = \frac{1}{N^2}\sum_{i=1}^{N}\sum_{j=1}^{N}\mathbf{z}^T\mathbf{A}_{i,j}^T\mathbf{A}_{i,j}\mathbf{z}$, where $A_{i,j}$ is the grid incidence matrix achieved by the loss of connection between node i and j. Similarly, numerical observability under SPL is defined as $\gamma = \frac{1}{N}\sum_{i=1}^{N}\mathbf{z}_i^T\mathbf{A}^T\mathbf{A}\mathbf{z}_i$, where $\mathbf{z}_i$ is achieved by the loss of PMU placed at the i-th grid node. Redundancy overhead φ for all these cases is calculated as $\varphi = N - \gamma$, while the binary numerical observability is given as $\mathrm{sign}(\varphi)$, where $\mathrm{sign}(\cdot)$ denotes the signum function. The numerical observability is attained, represented by 'Yes' (Y), when $\varphi > 0$, whereas it evaluates to 'No' (N), when $\varphi \leq 0$.

From Table X we note that the numerical observability for all IEEE test systems under the considered grid situations, i.e., 'Normal', 'SPL', and 'SLL', increases with the network size. This implies that the proposed controllability-aware optimal PMU placement strategy imparts higher redundancy with the increase in system size even considering system adversities. This can be attributed to the considered estimation approach in the optimal PMU placement viewpoint, rendering efficient grid estimation under system perturbation and adversities. This ensures a robust system monitoring for networks of different size. Further, it is notable that the redundancy overhead is always greater than zero, which increases as the network size grows. This translates to the signum function evaluating to 1 for all the considered test systems under all system conditions. This also ensures that the system is always numerically observable, even under grid adversities, such as SPL and SLL, as demonstrated in cells mentioning 'Y' in Table X. Therefore, the proposed controlability-aware optimization strategy does not violate the numerical observability of the test systems under a wide variety of system conditions. Moreover, positive numerical observability, represented in Table X, reinforces the stability of the proposed PMU placement strategy and solution

from the standpoint of being able to observe every grid node.

Remark 15. *It is notable that, the aspect of numerical observability is specific to the state estimation model employed in an analysis. Since the research in this manuscript discusses a novel case of controllability in perturbed power networks (unreported thus far in the literature) using data from the optimally deployed PMUs having single input current channel, the numerical observability presented in the manuscript is based on this estimation model, i.e.,* (9)*.*

V. Concluding Remarks

This paper proposed a novel power grid monitoring instrumentation strategy for grid controllability under perturbed conditions, wherein for optimal PMU deployment estimation practical constraint of limited number of input current channels was considered. Line observability reward, node weight vector, and polynomial observability constraint were separately defined that capture a generic grid situation, wherein the grid controllability feature in the optimization was presented through a binary multiplier. An information-theoretic approach to robust grid estimation at PDC was used for a joint optimization formulation, resulting in perturbation-robust optimal PMU placement solution with a decrease in MMSE, and near-unity mutual information. The proposed grid monitoring instrumentation strategy gives a handle to define system node weights based on their degree of instability. Simulation of perturbation in different IEEE bus systems of varied size demonstrated that the minimum number of PMUs increases and their optimal PMU placement location vary to deal with the perturbed system conditions. It was also demonstrated that optimal PMU placement based on observability constraint alone is not sufficient to capture grid health under perturbation, i.e., in ensuring an error-bounded estimation of the grid attributes at the data collector in perturbed power networks.

Appendix

A. Proof of Lemma 1

Applying energy balance on link j-j_r, where $j \in A_i$, $r \in [1, \cdots, k_j]$, we have

$$\begin{aligned} v_j \sin(\omega t + \phi_j) =& v_{j_r} \sin(\omega t + \phi_{j_r}) \\ & - i_{j_r,j} z_{j_r,j} \sin\left(\omega t + \delta_{j_r,j} + \theta_{j_r,j}\right) \end{aligned} \tag{A1}$$

where $\omega = 2\pi f$ is the grid frequency, $z_{i,j} = \sqrt{r_{i,j}^2 + x_{i,j}^2}$ is the impedance of link i-j, $\delta_{i,j}$ is the load angle, and $\theta_{i,j} = \tan^{-1}\left(\frac{x_{i,j}}{r_{i,j}}\right)$ with $r_{i,j}$, and $x_{i,j}$ denoting the link resistance and reactance, respectively. Dividing (A1) by $z_{j_r,j}$ and adding it for all incident nodes we have

$$\begin{aligned} \sum_{r=1}^{k_j} \frac{v_j \sin(\omega t + \phi_j)}{z_{j_r,j}} =& \sum_{r=1}^{k_j} \frac{v_{j_r} \sin(\omega t + \phi_{j_r})}{z_{j_r,j}} \\ & - \sum_{r=1}^{k_j} i_{j_r,j} \sin\left(\omega t + \delta_{j_1,j} + \theta_{j_1,j}\right). \end{aligned} \tag{A2}$$

Applying Kirchoff's current law (KCL) at node j in (A2) we have $\sum_{r=1}^{k_j} \frac{v_j \sin(\omega t + \phi_j)}{z_{j_r,j}} = \sum_{r=1}^{k_j} \frac{v_{j_r} \sin(\omega t + \phi_{j_r})}{z_{j_r,j}}$. Introducing perturbation we get

$$\begin{aligned} & \sum_{r=1}^{k_j} \frac{(v_j + \Delta v_j) \sin(\omega t + \phi_j + \Delta\phi_j)}{z_{j_r,j}} \\ & = \sum_{r=1}^{k_j} \frac{(v_{j_r} + \Delta v_{j_r}) \sin(\omega t + \phi_{j_r} + \Delta\phi_{j_r})}{z_{j_r,j}}. \end{aligned} \tag{A3}$$

Under small voltage perturbations [48], (A3) is linearized as

$$\begin{aligned} & \{\Delta v_j \sin(\omega t + \phi_j) + v_j \cos(\omega t + \phi_j)\Delta\phi_j\} \sum_{r=1}^{k_j} \frac{1}{z_{j_r,j}} \\ & = \sum_{r=1}^{k_j} \frac{\Delta v_{j_r} \sin(\omega t + \phi_{j_r})}{z_{j_r,j}} + \frac{v_{j_r} \cos(\omega t + \phi_{j_r})\Delta\phi_{j_r}}{z_{j_r,j}}. \end{aligned} \tag{A4}$$

Re-arranging (A4), we get

$$\mathbf{D}_j^T \begin{bmatrix} \Delta v_j \\ \Delta\phi_j \end{bmatrix} = \sum_{r=1}^{k_j} \mathbf{E}_{j_r}^T \begin{bmatrix} \Delta v_{j_r} \\ \Delta\phi_{j_r} \end{bmatrix} \frac{1}{\sum_{r=1}^{k_j} \frac{1}{z_{j_r,j}}} \tag{A5}$$

where $\mathbf{D}_j = \left[\sin(\omega t + \phi_j),\ v_j \cos(\omega t + \phi_j)\right]^T$ and $\mathbf{E}_{j_r}^T = \left[\frac{\sin(\omega t + \phi_{j_r})}{z_{j_r,j}},\ \frac{v_{j_r} \cos(\omega t + \phi_{j_r})}{z_{j_r,j}}\right]^T$. From the idea of small signal stability, we know that the voltage angle change relates to the machine rotor inertia, which is very small owing to high inertia in rotating parts. Therefore, from (A5) we get

$$\Delta v_j = \sum_{r=1}^{k_j} \frac{\sin(\omega t + \phi_{j_r}) z_{j_r,j}^{-1} \Delta v_{j_r}}{\sin(\omega t + \phi_j) \sum_{r=1}^{k_j} z_{j_r,j}^{-1}}. \tag{A6}$$

Let the instability grid node voltage change be Δv_0, such that $\Delta v_{j_r} = \alpha_{j_r} \Delta v_0$, where α_{j_r} is a constant of multiplication. Substituting this in (A6), we get

$$\omega_j = \frac{\Delta v_0}{\Delta v_j} = \frac{\sin(\omega t + \phi_j) \sum_{r=1}^{k_j} z_{j_r,j}^{-1}}{\sum_{r=1}^{k_j} \sin(\omega t + \phi_{j_r}) z_{j_r,j}^{-1} \alpha_{j_r}}. \tag{A7}$$

Note. *The expressions* (A1) *and* (A2) *are based on the theory of energy and charge balance, i.e., Kirchoff's voltage and current law, respectively. Since all physical systems must follow these properties, adhering to these principles provides guarantee of their physical realizability. Further, mathematical validity of the usage of perturbation theory in* (A3)-(A7) *stems from the utilization of Taylor's series.*

B. Proof of Lemma 2

Using (9), we formulate the performance metric as $V(\mathbf{z}) = \frac{1}{2} w(\mathbf{z})^T w(\mathbf{z})$. Differentiating V with respect to θ we have

$$\hat{\theta} = (H^T(\mathbf{z}) H(\mathbf{z}))^{-1} H(\mathbf{z})^T m(\mathbf{z}) \tag{B1}$$

Re-substituting $m(\mathbf{z})$ in (B1) we get

$$\begin{aligned} \hat{\theta} =& \overline{\theta} + \mathbb{E}\left[(H^T(\mathbf{z}) H(\mathbf{z}))^{-1} H(\mathbf{z})^T\right] (m(\mathbf{z}) - \overline{H}(\mathbf{z})\overline{\theta}) \\ =& \overline{\theta} + R_{m(\mathbf{z})\theta}^T R_{m(\mathbf{z})}^{-1} (m(\mathbf{z}) - \overline{H}(\mathbf{z})\overline{\theta}). \end{aligned} \tag{B2}$$

Expanding (B2) we get $\hat{\theta} = \overline{\theta} + R_\theta H(\mathbf{z})^T \left(\overline{H}(\mathbf{z}) R_\theta \overline{H}(\mathbf{z})^T + R_{w(\mathbf{z})}\right)^{-1} (m(\mathbf{z}) - \overline{H}(\mathbf{z})\overline{\theta})$. Using the definition for MSE as

defined before, and following (B2) we get

$$\begin{aligned} R_e(\mathbf{z}) =& R_\theta - R_{z(\mathbf{x})\theta}^T R_{z(\mathbf{x})}^{-1} R_{z(\mathbf{x})\theta} \\ =& R_\theta - R_\theta H(\mathbf{x})^T \left(H(\mathbf{x}) R_\theta \overline{H}(\mathbf{x})^T + R_{w(\mathbf{x})} \right)^{-1} \overline{H}(\mathbf{x}) R_\theta \\ \overset{(Aa)}{=}& \left(R_\theta^{-1} + \overline{H}(\mathbf{x})^T R_{w(\mathbf{x})}^{-1} \overline{H}(\mathbf{x})^T \right)^{-1} \\ =& \left(R_\theta^{-1} + \sum_{j=1}^{S} H_{k_j}^T R_{wk_j}^{-1} H_{k_j} \right)^{-1}. \end{aligned}$$

where equality (Aa) results from Woodbury matrix identity.

C. Proof of Lemma 3

It is notable that $z_i^\beta \leq z_i \ \forall \ z_i \in [0,1]$, so $\phi(\mathbf{z}) \leq \sum_{i\in\mathscr{N}} z_k = S \ \forall \mathbf{z} \in \text{Poly}(\mathscr{D}_R)$. Therefore, constraint $\mathbf{C}_1$ forces $\phi(\mathbf{z}) = R$, which is possible iff $z_i^\beta = z_i$, $i \in \mathscr{N}$, i.e., $z_k \in \{0,1\}$, $i \in \mathscr{N}$, implying $\mathbf{z} \in \mathscr{D}_R$.

REFERENCES

[1] P. Kundur, "Power system stability," *Power system stability and control*, 2007.

[2] A. K. Mandal, A. Malkhandi, S. De, N. Senroy, and S. Mishra, "A multipath model for disturbance propagation in electrical power networks," *IEEE Trans. Circuits Syst. II: Express Briefs*, pp. 1–1, 2022.

[3] L. Huang, J. Coulson, J. Lygeros, and F. Dörfler, "Decentralized data-enabled predictive control for power system oscillation damping," *IEEE Trans. Control Syst. Technol.*, vol. 30, no. 3, pp. 1065–1077, 2021.

[4] A. S. Musleh, S. Muyeen, A. Al-Durra, I. Kamwa, M. A. Masoum, and S. Islam, "Time-delay analysis of wide-area voltage control considering smart grid contingences in a real-time environment," *IEEE Trans. Ind. Informat.*, vol. 14, no. 3, pp. 1242–1252, 2018.

[5] Y. Ma, Q. Huang, Z. Zhang, and D. Cai, "Application of multisynchrosqueezing transform for subsynchronous oscillation detection using PMU data," *IEEE Trans. Ind. App.*, vol. 57, no. 3, pp. 2006–2013, 2021.

[6] A. K. Mandal and S. De, "Analysis of wireless communication over electromagnetic impulse noise channel," *IEEE Trans. Wireless Commun.*, pp. 1–1, 2022.

[7] S. Almasabi and J. Mitra, "Multistage optimal PMU placement considering substation infrastructure," *IEEE Trans. Ind. App.*, vol. 54, no. 6, pp. 6519–6528, 2018.

[8] L. Sun, T. Chen, X. Chen, W. K. Ho, K.-V. Ling, K.-J. Tseng, and G. A. Amaratunga, "Optimum placement of phasor measurement units in power systems," *IEEE Trans. Instrum. Meas.*, vol. 68, no. 2, pp. 421–429, 2018.

[9] Y. Li, J. Li, and L. Wu, "A novel integer linear programming based optimal PMU placement model," in *Proc. North American Power Symposium (NAPS)*. IEEE, 2018, pp. 1–6.

[10] C. D. Patel, T. K. Tailor, S. K. Shukla, S. Shah, and S. N. Jani, "Steiner tree-based design of communication infrastructure with co-optimizing the PMU placement for economical design of WAMS," *IEEE Trans. Instrum. Meas.*, vol. 71, pp. 1–11, 2022.

[11] M. Korkali and A. Abur, "Placement of PMUs with channel limits," in *2009 IEEE power & energy society general meeting*. IEEE, 2009, pp. 1–4.

[12] M. Korkali and A. Abur, "Impact of network sparsity on strategic placement of phasor measurement units with fixed channel capacity," in *in Proc. IEEE Int. Symp. Circuits Syst.* IEEE, 2010, pp. 3445–3448.

[13] M. Korkali, "Robust wide-area fault visibility and structural observability in power systems with synchronized measurement units," *Advances in Electric Power and Energy: Static State Estimation*, pp. 209–230, 2020.

[14] A. K. Mandal and S. De, "Joint optimal pmu placement and data pruning for resource efficient smart grid monitoring," *IEEE Trans. Power Syst.*, pp. 1–11, 2023.

[15] T. K. Maji and P. Acharjee, "Multiple solutions of optimal PMU placement using exponential binary PSO algorithm for smart grid applications," *IEEE Trans. Indus. Appl.*, vol. 53, no. 3, pp. 2550–2559, 2017.

[16] M. Shafiullah, M. I. Hossain, M. Abido, T. Abdel-Fattah, and A. Mantawy, "A modified optimal PMU placement problem formulation considering channel limits under various contingencies," *Measurement*, vol. 135, pp. 875–885, 2019.

[17] N. M. Manousakis and G. N. Korres, "Optimal PMU arrangement considering limited channel capacity and transformer tap settings," *IET Gener. Transm. Distrib.*, vol. 14, no. 24, pp. 5984–5991, 2020.

[18] X.-C. Guo, C.-S. Liao, and C.-C. Chu, "Probabilistic optimal PMU placements under limited observability propagations," *IEEE Syst. J.*, vol. 16, no. 1, pp. 767–776, 2021.

[19] N. P. Theodorakatos, A. P. Moschoudis, M. D. Lytras, and K. T. Kantoutsis, "Research on optimization procedure of PMU positioning problem achieving maximum observability based on heuristic algorithms," in *AIP Conf. Proc.*, vol. 2872, no. 1. AIP Publishing, 2023.

[20] M. K. Arpanahi, H. H. Alhelou, and P. Siano, "A novel multiobjective OPP for power system small signal stability assessment considering WAMS uncertainties," *IEEE Trans. Ind. Informat.*, vol. 16, no. 5, pp. 3039–3050, 2019.

[21] W. Li, D. Deka, M. Chertkov, and M. Wang, "Real-time faulted line localization and PMU placement in power systems through convolutional neural networks," *IEEE Trans. Power Syst.*, vol. 34, no. 6, pp. 4640–4651, 2019.

[22] M. Zhang, Z. Wu, J. Yan, R. Lu, and X. Guan, "Attack-resilient optimal PMU placement via reinforcement learning guided tree search in smart grids," *IEEE Trans. Informat. Foren. Secur.*, vol. 17, pp. 1919–1929, 2022.

[23] N. P. Theodorakatos, M. D. Lytras, A. P. Moschoudis, and K. T. Kantoutsis, "Implementation of optimization-based algorithms for maximum power system observability using synchronized measurements," in *AIP Conf. Proc.*, vol. 2872, no. 1. AIP Publishing, 2023.

[24] M. Elimam, Y. J. Isbeih, M. S. El Moursi, K. Elbassioni, and K. H. Al Hosani, "Novel optimal PMU placement approach based on the network parameters for enhanced system observability and wide area damping control capability," *IEEE Trans. Power Syst.*, vol. 36, no. 6, pp. 5345–5358, 2021.

[25] A. N. Samudrala, M. H. Amini, S. Kar, and R. S. Blum, "Sensor placement for outage identifiability in power distribution networks," *IEEE Trans. Smart Grid*, vol. 11, no. 3, pp. 1996–2013, 2019.

[26] M. H. R. Koochi, P. Dehghanian, and S. Esmaeili, "PMU placement with channel limitation for faulty line detection in transmission systems," *IEEE Trans. Power Deliv.*, vol. 35, no. 2, pp. 819–827, 2019.

[27] M. Ghamsari-Yazdel, M. Esmaili, F. Aminifar, P. Gupta, A. Pal, and H. Shayanfar, "Incorporation of controlled islanding scenarios and complex substations in optimal WAMS design," *IEEE Trans. Power Syst.*, vol. 34, no. 5, pp. 3408–3416, 2019.

[28] M. H. R. Koochi and M. H. Hemmatpour, "A general PMU placement approach considering both topology and system aspects of contingencies," *Int. J. Electr. Power Energy Syst.*, vol. 118, p. 105774, 2020.

[29] S. Almasabi and J. Mitra, "A fault-tolerance based approach to optimal PMU placement," *IEEE Trans. Smart Grid*, vol. 10, no. 6, pp. 6070–6079, 2019.

[30] Z. M. Ali, S.-E. Razavi, M. S. Javadi, F. H. Gandoman, and S. H. Abdel Aleem, "Dual enhancement of power system monitoring: Improved probabilistic multi-stage PMU placement with an increased search space & mathematical linear expansion to consider zero-injection bus," *Energies*, vol. 11, no. 6, p. 1429, 2018.

[31] D.-I. Kim, A. White, and Y.-J. Shin, "PMU-based event localization technique for wide-area power system," *IEEE Trans. Power Syst.*, vol. 33, no. 6, pp. 5875–5883, 2018.

[32] A. N. Samudrala, M. H. Amini, S. Kar, and R. S. Blum, "Distributed outage detection in power distribution networks," *IEEE Trans. Smart Grid*, vol. 11, no. 6, pp. 5124–5137, 2020.

[33] J. Segundo-Ramirez, A. Bayo-Salas, M. Esparza, J. Beerten, and P. Gómez, "Frequency domain methods for accuracy assessment of wideband models in electromagnetic transient stability studies," *IEEE Trans. Power Deliv.*, vol. 35, no. 1, pp. 71–83, 2020.

[34] A. K. Mandal, S. De, and B. K. Panigrahi, "Grid controllability aware optimal placement of pmus with limited input current channels," in *Proc. IEEE Int. Conf. Ener. Technol. Future Grids (ETFG)*. IEEE, 2023, pp. 1–6.

[35] *Reliability Guideline: PMU Placement and Installation*, North American Electric Reliability Corporation, 2016. [Online]. Available: https://www.nerc.com/comm/RSTC_Reliability_Guidelines/Reliability\%20Guideline\%20-\%20PMU\%20Placement.pdf

[36] *A Guide for PMU Installation, Commissioning and Maintenance. Part II. PMU Installation Procedures*, North American SynchroPhasor Initiative (NASPI), Performance & Standards Task Team (PSTT), 2007.

[Online]. Available: https://www.naspi.org/sites/default/files/reference_documents/81.pdf

[37] *A Guide for PMU Installation, Commissioning and Maintenance. Part I. PMU Acceptance Test Checklist for Connecting to TVA SuperPDC*, North American SynchroPhasor Initiative (NASPI), Performance Requirements Task Team (PRTT), 2009. [Online]. Available: https://www.naspi.org/sites/default/files/reference_documents/84.pdf

[38] *NASPI Synchrophasor Starter Kit*, North American SynchroPhasor Initiative (NASPI), 2015. [Online]. Available: https://www.naspi.org/sites/default/files/reference_documents/4.pdf

[39] "IEEE standard for synchrophasor measurements for power systems," *IEEE Std C37.118.1-2011 (Revision of IEEE Std C37.118-2005)*, pp. 1–61, 2011.

[40] D. P. Kothari and I. Nagrath, *Modern power system analysis*. Tata McGraw-Hill Education, 2003.

[41] F. Aminifar, M. Fotuhi-Firuzabad, M. Shahidehpour, and A. Khodaei, "Probabilistic multistage PMU placement in electric power systems," *IEEE Trans. Power Deliv.*, vol. 26, no. 2, pp. 841–849, 2010.

[42] A. G. Phadke and J. S. Thorp, *Synchronized phasor measurements and their applications*. Springer, 2008, vol. 1.

[43] A. Hassanat, K. Almohammadi, E. Alkafaween, E. Abunawas, A. Hammouri, and V. S. Prasath, "Choosing mutation and crossover ratios for genetic algorithms—a review with a new dynamic approach," *Information*, vol. 10, no. 12, p. 390, 2019.

[44] S. Mirjalili and S. Mirjalili, "Genetic algorithm," *Evolutionary algorithms and neural networks: Theory and applications*, pp. 43–55, 2019.

[45] M. Qasim Khan, M. Mohamud Ahmed, and A. M. Haidar, "An accurate algorithm of PMU-based wide area measurements for fault detection using positive-sequence voltage and unwrapped dynamic angles," *Measurement*, vol. 192, p. 110906, 2022. [Online]. Available: https://www.sciencedirect.com/science/article/pii/S0263224122001877

[46] A. J. Wood, B. F. Wollenberg, and G. B. Sheblé, *Power generation, operation, and control*. John Wiley & Sons, 2013.

[47] N. M. Manousakis and G. N. Korres, "Optimal allocation of phasor measurement units considering various contingencies and measurement redundancy," *IEEE Trans. Instrum. Meas.*, vol. 69, no. 6, pp. 3403–3411, 2020.

[48] R. Zhu, Z. Chen, Y. Tang, F. Deng, and X. Wu, "Dual-loop control strategy for DFIG-based wind turbines under grid voltage disturbances," *IEEE Trans. Power Electron.*, vol. 31, no. 3, pp. 2239–2253, 2016.